Front. Phys. 13(4), 138114 (2018)
https://doi.org/10.1007/s11467-018-0795-x

REVIEW ARTICLE

Environmental engineering of transition metal dichalcogenide optoelectronics

Trevor LaMountain, Erik J. Lenferink, Yen-Jung Chen, Teodor K. Stanev, Nathaniel P. Stern†

Department of Physics and Astronomy, Northwestern University, Evanston, Illinois 60208, USA
Corresponding author. E-mail: †*n-stern@northwestern.edu*
Received February 26, 2018; accepted April 9, 2018

The explosion of interest in two-dimensional van der Waals materials has been in many ways driven by their layered geometry. This feature makes possible numerous avenues for assembling and manipulating the optical and electronic properties of these materials. In the specific case of monolayer transition metal dichalcogenide semiconductors, the direct band gap combined with the flexibility for manipulation of layers has made this class of materials promising for optoelectronics. Here, we review the properties of these layered materials and the various means of engineering these properties for optoelectronics. We summarize approaches for control that modify their structural and chemical environment, and we give particular detail on the integration of these materials into engineered optical fields to control their optical characteristics. This combination of controllability from their layered surface structure and photonic environment provide an expansive landscape for novel optoelectronic phenomena.

Keywords transition metal dichalcogenides, optoelectronics, van der Waals materials, heterostructures, excitons

PACS numbers 68.35.bg, 78.20.-e, 73.21.-b, 81.07.-b

Contents

*Special Topic: Graphene and other Two-Dimensional Materials (Eds. Daria Andreeva, Wencai Ren, Guangcun Shan & Kostya Novoselov).

Frontiers of Physics

1 Introduction

A key ingredient in device design for optical and electronic applications is the ability to intentionally control material properties. Classic examples include tailoring semiconductor confinement for lasing, photovoltaic, and sensing applications [1–3], controlling doping and defects for high mobility transistors [4], exploiting metal plasmons for enhanced absorption [5], and engineering of magnetic and spin properties for logic and memory [6, 7]. Although the idea of controlling the environment of materials is an old one, the emergence of a wide class of layered van der Waals (vdW) materials is revealing new opportunities for designing devices by controlling the structural and electromagnetic environment of materials at the atomic scale.

Since the isolation of graphene, layered vdW materials in which individual crystal planes are held together by van der Waals forces have attracted interest due to their intriguing low-dimensional properties of single layers and the ability to design more complex heterostructures through layer stacking [11–14]. In particular, the group VI layered transition metal dichalcogenides (TMDs) such as MoS_2 and WSe_2 and their related compounds have been identified as being especially useful for optoelectronics because, unlike graphene, they can be direct bandgap semiconductors in the single layer limit. This combination of favorable optical properties and the layer-dependent two-dimensional electronic structure creates a highly tunable material platform that has seen incredible advances across several distinct disciplines, exemplified by new discoveries in low-dimensional electronic physics [15–20], high-performance electrical devices [21–24], classical [25–29] and quantum [10, 30–33] optical devices, plasmonics [34–38], polaritonics [39–42] and others. Looking specifically at optoelectronics, these desirable traits have led to rapid development of photodetectors [43], solar cells [44, 45], light-emitting diodes [46–48], excitonic lasers [49, 50] and even more unique devices relying on the emergent properties of monolayer semiconductors [51–53].

Underlying this broad exploration in both fundamental and device applications is the remarkable tunability of these materials provided by their layered structure. Since these two-dimensional (2D) materials are effectively all surface, they are extremely sensitive to their environments. This fact, both a feature and a bug, manifests throughout the many achievements in this class of materials. In this manuscript, we review the opportunities presented by environmental engineering of TMDs for optoelectronics. We introduce some of the methods that have been developed to tune optical properties of single-layer TMD materials, focusing on the unique features that set them apart from other nanomaterials. We place a particular emphasis on reviewing how engineering the optical environment can manipulate electronic properties of these materials when integrated with photonics. The rapid development in recent years of this optical approach complements the structural and electronic engineering tools already widely available to control layered semiconductor optoelectronics.

2 2D semiconductors – monolayer transition metal dichalcogenides

In this section we introduce the unique structural, optical, and electronic properties of transition metal dichalcogenide monolayers that make these materials an intriguing platform for optoelectronics. We discuss band structures, crystal symmetries, excitons, emergent spin and valley degrees of freedom, optical selection rules, and coherent optical effects in TMDs. Although these properties are covered extensively in numerous recent reviews [54–57], sufficient detail is included here to appreciate the relevant features discussed in this article.

2.1 Excitonic optical properties

Monolayers of group VI TMDs are a class of direct bandgap semiconductors [60] consisting of three atomic layers in a trigonal prismatic arrangement. In this review we will focus solely on the TMDs of the chemical form MX_2 where M is Mo or W and X is S or Se. The reduced vertical dimensionality of these quasi-2D crystals leads to a significant reduction in dielectric screening. Consequently, photoexcited electrons and holes in these materials experience a strong Coulomb interaction, leading to the formation of excitons with large binding energies on the order of hundreds of meV and small Bohr radii in the range of several nanometers [61]. These tightly-bound excitons, with transition energies below the quasiparticle bandgap, dominate the optical response of TMDs even at room temperature. The optical bandgaps of these materials lie in the visible and near infrared spectrum, shown in Fig. 1(a). While a spectrum of Rydberg-like excited exciton states exist in these materials [62], the low-energy 1s state typically plays the largest role in linear absorption and emission processes. Within the 1s state there are two subspecies of neutral excitons corresponding to the A and B band transitions [60] shown in Fig. 1(c). In this review we typically focus on the lowest-energy A exciton.

This optical structure of monolayer TMDs provides an intriguing platform for exploring and controlling excitonic physics because of the reduced screening and environmental sensitivity of these layered materials. For

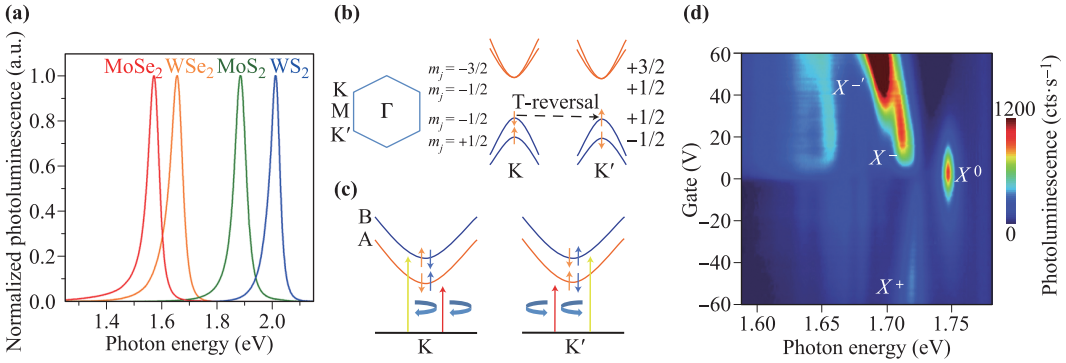

Fig. 1 Excitonic effects in monolayer TMDs. **(a)** Room temperature photoluminescence spectra of monolayer TMDs illustrating the range of optical bandgaps. **(b)** Illustration of monolayer TMD Brillouin zone and band structure at the K and K' valleys. **(c)** Band structure of bright excitons the K and K' valleys. **(d)** Electrostatic gating dependence of the photoluminescence of monolayer WSe_2 at low temperature with the exciton species labeled. Figures reproduced with permission from: (a, b) Ref. [8], Copyright © 2012 American Physical Society; (c) Ref. [9], Copyright © 2016 American Chemical Society; (d) Ref. [10], Copyright © 2013 Nature Publishing Group.

example, the absorption and photoluminescence spectra also show features corresponding to charged excitons (trions) made from a photoexcited exciton and a resident charge carrier [63]. The spectral contributions of the positively and negatively charged and neutral excitons can be tuned by electrostatic gating. In monolayer MoS_2 the luminescence can only be shifted between the neutral X and negatively charged X^- excitons [63] due to the intrinsic n-doping of the material, but in ambipolar monolayers such as WSe_2, the emission of both positively and negatively charged trion species may be controllably activated [10] as shown in Fig. 1(d). Since excitons and trions have non-zero out-of-plane dipole moments, the gating field can tune the emission energies via the Stark effect [64]. This excitonic Stark shift has also been observed in more complex TMD multilayers, which can support interlayer excitons [65, 66]. With charge distribution spanning distinct material layers, the stronger out-of-plane dipole moment results in a more pronounced Stark shift. Finally, we note that electrostatic gating can be used to reduce the spectral weight of broad, lower-energy emission arising from to the presence of defect states [67]. These tunable features, all available at room temperature, demonstrate how electric fields can offer a simple knob for controlling excitonic properties in monolayer TMDs.

2.2 Spin-valley physics

Besides the strong excitonic features of monolayer TMDs, their 2D crystal symmetries combined with spin-orbit coupling give rise to more exotic optoelectronic features. Specifically, for the common 2H TMD polytype, the direct bandgap occurs at two degenerate valleys located at the corners of the hexagonal Brillouin zone [68] labeled K and K' [Fig. 1(b)], in analogy to the semimetal graphene. The valley index can effectively label charge carriers near the Fermi level as they are well-separated in momentum space. In contrast to graphene, the combination of strong spin-orbit coupling originating in the transition metal d orbitals and the inversion asymmetry of the lattice results in a spin splitting of the conduction and valence bands with opposite splitting at the two valleys (as required from time-reversal symmetry [68]). This splitting is far more pronounced for holes [69] and results in a locking between spin and valley [70]; in order to scatter to the opposite valley and conserve energy, a carrier's spin must flip simultaneously, which typically requires an atomically-sharp magnetic defect [8]. However, the valley and spin polarization of these locked states are limited in practice by a fast electron-hole exchange interaction that can generate rapid valley depolarization [71].

A consequence of the inversion asymmetry is that the carriers in the two valleys are inherently inequivalent and possess valley-contrasting magnetic moment and Berry curvature [72]. The former results in valley-dependent optical selection rules with opposite valleys coupling to opposite circular polarizations of light [68] as depicted in Fig. 1(c). The latter causes valley Hall effects with longitudinal valley currents producing transverse charge currents and vice-versa [17, 73]. Since these selection rules make the valleys optically-addressable through circularly-polarized light, the index label can function as an emergent pseudospin with similar opportunities for manipulation as traditional spin. While the idea of manipulating electronic states in different valleys is not new [74], the optical selection rules in monolayer TMDs with an appreciable intrinsic direct bandgap and strong excitonic features provide the means to translate valley pseudospin control to layered optoelectronics.

3 Optoelectronics with TMDs

With visible frequency bandgaps and thicknesses at the atomic limit, monolayer TMDs have seen considerable interest for flexible optoelectronic devices such as photovoltaics [54]. A number of recent articles provide an in-depth review of the wide array of current and developing device applications using TMDs [75–77]. Here, rather than focusing on the devices themselves, we highlight some of the novel mechanisms important to TMD optoelectronics, specifically, free carrier generation and valley-sensitive effects in devices.

3.1 Free carrier generation

Conventional optoelectronics typically require the generation of free carriers, which can present a challenge for exciton-dominated materials like TMDs. Early research focused on n-doped monolayer MoS_2 devices, and it was found that the photoresponse is primarily a convolution of slow photovoltaic and fast photoconductive effects [78]. Spatially-resolved measurements have revealed that the photocurrents are only appreciably generated when the Schottky barriers of metal contacts, which enable the dissociation of excitons into free carriers, are illuminated [79]. Band offsets in monolayer/multilayer MoS_2 homojunctions have also been found to enable free carrier generation [20, 80, 81]. Local electrostatic gating enables creation of monolayer p–n diodes, allowing for more efficient light harvesting and light-emitting diodes. For example, monolayer WSe_2 has been used to realize diodes [45, 47, 48] which exhibit a photoresponse spatially localized to the p–n interface and electroluminescence that spectrally matches the monolayer's photoluminescence. With free carrier generation in TMD devices becoming well-understood, more unique optoelectronic systems can be developed which can exploit the spin and valley properties of TMDs.

3.2 Valley-sensitive optoelectronics

As a result of the valley-dependent optical selection rules, energetically degenerate excitons localized at the K and K' valleys emit opposite circular polarizations of light. This has been experimentally confirmed for various TMDs in low-temperature circularly-polarized photoluminescence experiments in which the monolayer is excited with one polarization of light and the valley polarization $\mathcal{P}$ of excitons can be extracted from the circularly-polarized luminescence [8, 82, 83]. An example circular photoluminescence measurement of monolayer WSe_2 is shown in Fig. 2(a). Reported values vary between the TMD materials and measurement conditions (particularly the energy detuning of the pump excitation) but valley polarizations exceeding 50% are common for both charged and neutral excitons [63]. This suggests valley lifetimes on the order of the exciton recombination lifetime from a simple exciton depolarization rate model,

$$\mathcal{P} = \frac{1}{1 + 2\tau_r/\tau_v}, \tag{1}$$

where τ_r and τ_v are the exciton decay rate and valley lifetimes respectively. Time-resolved photoluminescence measurements at cryogenic temperatures have revealed that τ_r for the A exciton lies in the picosecond regime

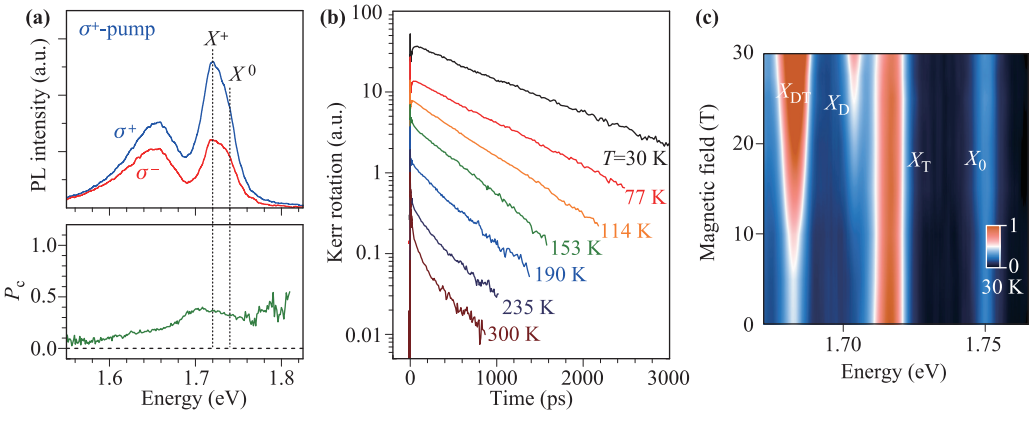

Fig. 2 Valley-dependent optical properties of TMDs. **(a)** Low temperature circularly-polarized photoluminescence collected from a WSe_2 monolayer with the neutral and charged trion peaks labeled. The pump polarization is σ_+. The lower energy broad peak is attributed to localized defect-bound excitons. The lower panel shows the polarization. **(b)** Time-resolved Kerr rotation from the same WSe_2 sample as in (a) probed at the charged exciton energy. **(c)** Photoluminescence spectra of a WSe_2 monolayer as a function of the in-plane magnetic field at a temperature of 30 K with the bright neutral and charged excitons and their corresponding dark states labeled. Figures reproduced with permission from: (a, b) Refs. [58], Copyright © 2015 Nature Publishing Group, licensed under CC BY; (c) Ref. [59], Copyright © 2017 Nature Publishing Group.

[84–88]. The correspondingly short τ_v has been confirmed for the neutral exciton using polarization-dependent time-resolved photoluminescence [85, 86]. The observed rapid valley depolarization has been explained as the result of the electron-hole exchange interaction. The valley depolarization of trions, however, is more subtle with both a fast initial decay similar to neutral excitons before a slow decay with a corresponding lifetime extending into the nanoseconds measured for monolayer WSe_2 [85].

Supplementing photoluminescence measurements, time-resolved Kerr rotation has been employed extensively to measure spin and valley lifetimes in monolayer TMDs. While in undoped monolayers the spin/valley lifetime is limited to the picosecond regime [89], measurements in doped monolayers have revealed far longer lifetimes extending well into the nanosecond range for the various TMDs at cryogenic temperatures [58, 90–92] [Fig. 2(b)]. These extended polarization-sensitive decays reflect the lifetimes of free carriers. For example, a recent study on monolayer WSe_2 used a gate bias to probe both types of free carriers, measuring a hole valley lifetime of 2 μs and an electron spin lifetime of 160 ns [93]. Achieving comparably long lifetimes for excitons is desirable for harnessing valley pseudospin in optoelectronic devices, which may be attainable by engineering couplings between monolayer TMDs and their surrounding environments.

Breaking the energy degeneracy of excitons at the K and K' valleys is a potential mechanism for manipulating pseudospin-sensitive optics. Similar to traditional spin, out-of-plane magnetic fields induce a valley-dependent Zeeman shift of the exciton transitions due to the intrinsic valley magnetic moment. Magnetic field valley splitting has been observed in monolayers of WSe_2 [94, 95] and $MoSe_2$ [96, 97] at cryogenic temperatures using circularly polarized photoluminescence. The measured g factors generally match the theoretical value of 4 from expected from the hole's d-orbital. In-plane magnetic fields, conversely, do not couple to the valley pseudospin of carriers but may cause spin precession. This has been utilized to discriminate between spin and valley related phenomena; an effect that is robust to in-plane magnetic fields such as circular polarized photoluminescence can be generally attributed to carrier valley dynamics [82]. The spin precession induced by in-plane fields is also necessary to optically probe species of dark excitons [59, 98] composed of electron-hole pairs with spin-forbidden dipole transitions. At high magnetic fields the dark excitons brighten and become spectrally distinct in analogy to the A and B bright excitons as shown in Fig. 2(c). The rich and tunable spin-valley physics in monolayer TMDs demonstrate how polarization-sensitive optical properties can be tailored for specific applications.

3.2.1 *Valley coherence*

Quantum superpositions of valley excitons enable manipulation of excitations that coherently span multiple valleys, suggesting applications in valleytronics and information processing. Linearly polarized light, which contains equal components of left- and right-circular polarization, can generate intervalley coherence of excitons in the K and K' valleys in WSe_2 [10, 99–101], WS_2 [102], and MoS_2 [103, 104]. This coherence was first detected through the observation of linearly-polarized photoluminescence where the primary axis of emission corresponds to the excitation polarization [10]. The agreement between excitation and emission orientation suggests that intervalley coherence persists on a timescale comparable to recombination. The valley coherence time (∼ 100 fs in WSe_2) has been directly measured using polarization-resolved two-dimensional coherent spectroscopy [105]. As with traditional circularly polarized luminescence, the short valley coherence time is typically attributed to the electron-hole exchange interaction that couples the two valleys and allows rapid decoherence [71, 105].

In analogy to spin, coherent valley states can be manipulated by breaking the energy degeneracy of the valley exciton transitions [100–102]. When the transition energy of the two valleys is unequal, a phase difference accumulates between the two components of the coherent superposition. This is typically represented as a rotation of the spin/pseudospin state on the Bloch sphere [Fig. 3(a)] and manifests as a rotation in the axis of linearly polarized emission [Fig. 3(b)]. Such rotations have been demonstrated in the steady-state using out-of-plane magnetic fields and continuous-wave excitation [100, 102]. The steady-state detectability of these effects is largely due to the fact that valley coherence can be generated and detected using off-resonant

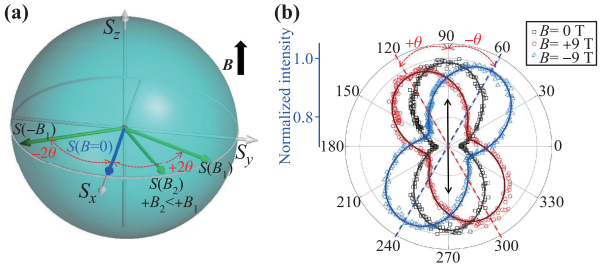

Fig. 3 Valley coherence. **(a)** Bloch sphere used to represent coherent superpositions of valley states. **(b)** Linear polarization dependence of photoluminescence with and without magnetic field. Black arrow shows orientation of linearly-polarized excitation. Angle of rotation θ corresponds to half the rotation on the Bloch sphere. Figure reproduced with permission from Ref. [100], Copyright © 2016 American Physical Society, licensed under CC BY.

light [10, 99, 100]. Coherent valley rotations have also been demonstrated using all-optical ultrafast "pseudo-magnetic fields", a topic that is explored in detail in Section 5.3.2.

3.2.2 Photoexcited valley-sensitive devices

The valley index of photoexcited charge carriers in a monolayer TMD can be used for electronic devices. The valley-dependent Berry curvature in monolayer TMDs manifests as a valley-contrasting mobility transverse to the applied electric field. If a valley-polarized current is generated in a monolayer Hall bar device, a complimentary charge current is also generated, resulting in a Hall voltage in the absence of any magnetic field. This valley Hall effect was first measured in n-doped monolayers of MoS_2 [73] at cryogenic temperatures when pumped by circularly-polarized light with energy slightly above the bandgap. The origin of the transverse voltage was ascribed to valley-polarized electrons generated when the Schottky barriers at the source and drain contacts were illuminated. More recently the valley Hall effect was measured in n-doped monolayer WS_2 where spectrally-resolved spatial mapping revealed that both valley-polarized free carriers and trions contribute the measured Hall voltage [106]. These conclusions are further bolstered by spatially-resolved measurements of valley-polarized exciton diffusion in monolayer MoS_2 [107]. In this experiment a linearly polarized pump was centered at one edge of a narrow monolayer, as shown in Fig. 4(a, b), resulting in largely unidirectional thermal and chemical potential gradients. Polarization-resolved spatial mapping of the photoluminescence revealed that excitons in the two valleys experience opposite transverse diffusion as can be see in Fig. 4(c), demonstrating an excitonic valley Hall effect.

The complimentary creation of a transverse valley current from a longitudinal charge current has also been observed in n-doped MoS_2 monolayers [108] and bilayers [17] with inversion symmetry broken via electrostatic gating. By electrically biasing monolayers at cryogenic temperatures, regions of local valley accumulation are established at the edges of the monolayer conducting channel that can be measured with spatially-resolved Kerr rotation in analogy to the spin Hall effect [109]. Extraction of the electron valley diffusion length scale remains difficult but with far longer valley lifetimes [93], hole-doped monolayers may offer a greater potential for probing free carrier valley diffusion length scales.

The circularly polarized photogalvanic effect (CPGE) has also been utilized to study the spin and valley dynamics of monolayer TMDs. As the effect only arises in systems with spatial inversion asymmetry, previous studies on the CPGE in graphene relied on an extrinsic symmetry breaking, i.e., the presence of the bottom dielectric substrate [110]. By contrast, monolayer TMDs constitute a natural platform for studies of the CPGE with spin-valley currents observed in monolayer MoS_2 as well as MoS_2 and WSe_2 electric-double-layer transistors at room temperature [111–113].

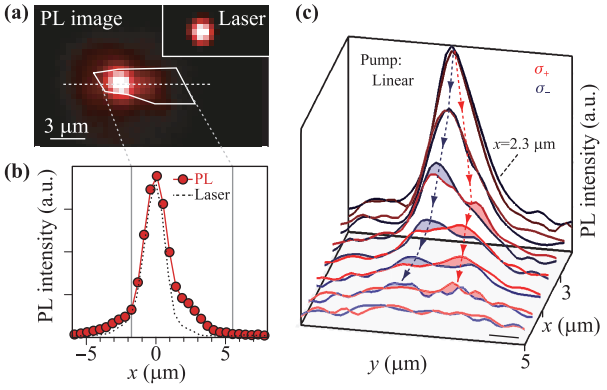

Fig. 4 Exciton valley Hall effect. **(a)** Spatial photoluminescence intensity map of a MoS_2 monolayer (outlined in white) used to observe the exciton valley Hall effect. The linearly polarized pump beam is fixed at one side of the monolayer and excitons diffuse along the x axis seen in the cross-sectional profile **(b)**. **(c)** Polarization-resolved photoluminescence intensity cross-sections taken along y spaced approximately 0.46 μm in x demonstrating transverse diffusion of valley-polarized excitons. Figure reproduced with permission from Ref. [107], Copyright © 2017 Nature Publishing Group.

4 Structural and electronic engineering of TMDs

Owing to their two-dimensional structure, the electronic and optical properties of monolayer TMDs are highly dependent on their surrounding environment [114–116]. This sensitivity can be exploited to engineer behavior for optoelectronics. In this section, we review recent progress in controlling monolayer TMD devices by modifying their surrounding material and electronic environments.

4.1 Surface modification

In contrast to conventional 3D bulk semiconductors, the exposed 2D surface of monolayer TMDs allows for significant modification of material properties using surface treatments. These can alter excitonic lifetimes, dope the underlying layer by charge transfer, and greatly enhance Raman signals. Examples of such treatments are functionalization with polar molecules such as phthalocyanines (Pc), pyridine, and pyrazine [43, 117–120], chemical layers such a rhodamine 6G and pentacene

[17, 121], and interfacing with quantum dots [122, 123]. As a particular example, Pc has been investigated by many groups for its charge transfer and Raman enhancement effects [118] and improvement of photodetectors [43, 124]. For chemical layer treatment, pentacene has been found to enable hole-transfer and long-lived charge separation [121, 125].

Interfacing TMDs with semiconductor quantum dots (QDs) has also attracted interest as a platform for novel optoelectronic devices that could exploit the high quantum efficiencies of quantum dots and the high carrier mobilities of TMDs [122, 126, 127]. For example, the energy transfer from CdSe QDs to monolayer TMDs extends the photoluminescence lifetime of excitons in TMDs [123]. This feature results from the ∼ns timescale decay of excitons in the quantum dots, which limits the rate of energy transfer from the QDs into the TMD. Consequently, the ∼ps scale photoluminescence signal in bare TMD is extended to nanoseconds in the composite system, demonstrating how mixed material heterostructures can be used to engineer dynamics in TMDs.

Another example of surface engineering for TMDs is the use of reparative chemisorption for photoluminescence enhancement (shown to reach near-unity), defect repair, and crystal vacancy filling [9, 128–131] [Fig. 5]. This type of chemisorption can be achieved using superacids, molecular surface treatments, and sulfur/selenide annealing. Because the vacancies are also electron donation centers, chemisorption can be leveraged for doping in TMD systems, providing control over carrier populations as well as trion and localized exciton optical emissions.

A variety of other surface treatments have been shown to effectively dope TMDs. Hole doping can be achieved with gold-chloride treatments [132], phosphorous implantation in vacancies [133], gold dressing [134], and boron-based oxidant treatments [135]. Electron doping has been demonstrated using alkali elements [136, 137], thin films of silicon nitride [138], and black phosphorous nanodots [139]. Many of these surface treatments are also completely reversible. For example, molecular hydrazine dopes TMDs through electron charge donation and the formation of sulfur vacancies, a process that can be completely undone by sulfur annealing [140].

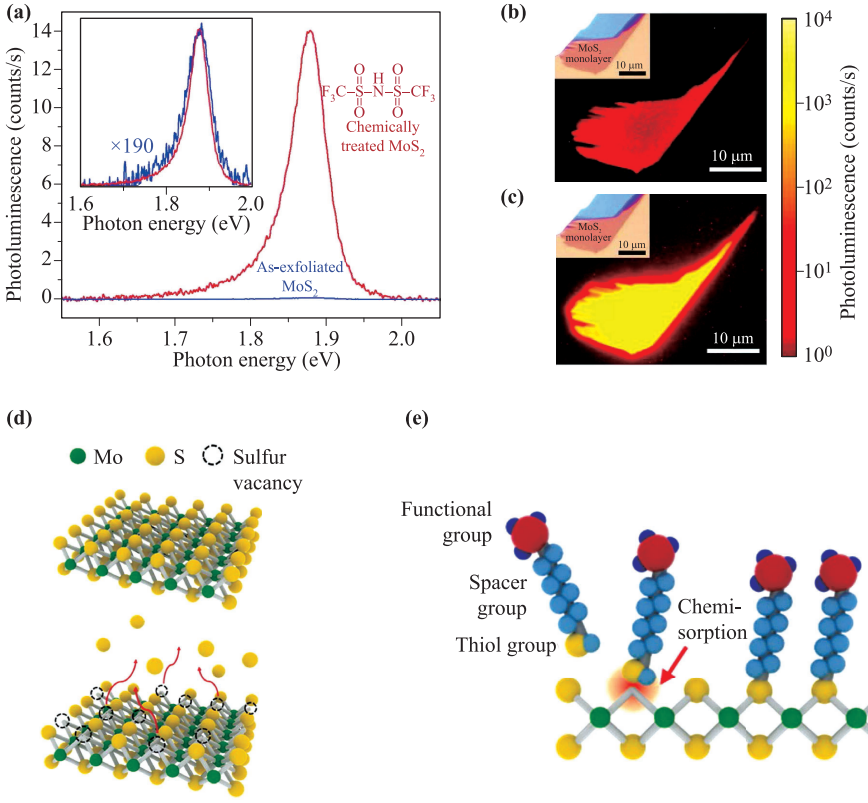

Fig. 5 Examples of surface engineering. **(a)** Near 200-times enhancement in MoS_2 PL after superacid treatment of the surface [128]. **(b, c)** Spatial comparison before and after superacid treatment showing enhancement over the entire MoS_2 flake. **(d)** Pristine MoS_2 layer (top) vs. a sulfur vacancy rich MoS_2 layer (bottom). **(e)** Sulfur vacancies treated by chemisorption [129]. Figures reproduced with permission from (a, c) Ref. [128], Copyright © 2015 American Association for the Advancement of Science; (d, e) Ref. [129], Copyright © 2015 American Chemical Society.

4.2 Layered heterostructures

One of the capabilities enabled by van der Waals materials is the ability to create composite materials with layer-by-layer stacking, providing atomic-scale control of the environment surrounding a given layer. These vdW heterostructures [11–13, 76] provide atomic-scale control of the surrounding environment that has been exploited for optoelectronics.

4.2.1 TMD-TMD heterostructures

Mixed-TMD heterostructures can help overcome the limitations of standalone TMDs. For example, a TMD heterostructure with a band offset between the two monolayer materials enables efficient charge separation that can help optoelectronic applications such as photosensing and light harvesting [143]. Lateral heterostructures created with multi-stage chemical vapor deposition operate nominally as p–n junctions, demonstrating current rectification and photocurrent generation at the interface [144]. Alternatively, vertical TMD heterostructures created with polymer transfer techniques boast an atomically sharp vdW interface with a larger coverage area for light absorption [145, 146]. An optical image of an example monolayer $MoSe_2/WSe_2$ vdW heterostructure is shown in Fig. 6(a). Two color pump-probe measurements of these vdW heterostructures have revealed ultrafast charge transfer times of 470 fs for a MoS_2/WSe_2 heterostructure [147], with a high degree of transfer efficiency. This quick charge transfer is favorable for photovoltaic applications as well as valley optoelectronics as it limits the valley depolarization of photoexcited excitons before dissociation. This has been demonstrated in a MoS_2/WSe_2 heterostructure where charge separation produced valley polarized resident holes in the WSe_2 with a valley lifetime of 40 μs at 10 K as measured by time-resolved Kerr rotation [148]. Measurements on $MoSe_2/WSe_2$ have also shown that spin/valley polarization can be conserved through the charge separation process [149] even for non-ideal twist angles between layers, demonstrating utility for valley-polarized free carrier generation.

Photoluminescence measurements of type-II vdW heterostructures such as $MoSe_2/WSe_2$, have revealed bright interlayer excitons when the twist angle between the two monolayers is close to 0° or 60° (determined using second harmonic generation) corresponding to AA and AB stacking, respectively [150–152]. The luminescence peak corresponding to the interlayer exciton lies several hundred meV below the intralayer exciton peaks from the two constituent materials [Fig. 6(b)]. It is strongly tunable with electrostatic gating due to the out-of-plane electric dipole moment [151, 153]. The luminescence energy of the interlayer exciton can also be modified by inserting a hexagonal boron nitride (h-BN) buffer between the two layers, though the exciton disappears after only a few layers of h-BN [150].

The twist angle dependence that limits interlayer exciton formation in TMD heterostructures is not just a technical hurdle; this feature can also be leveraged to tune the interaction between layers. For example, in TMD homostructures, which consist of deterministically stacked layers the same TMD material, coupling between layers can vary as a function of twist angle [154–156]. One consequence of this twist angle dependence is the recovery of valley-dependent optical selection rules in stacked bilayers of TMDs [157–159].

Remarkably, the recombination and valley lifetimes of these interlayer excitons as measured by time-resolved methods are long: tens to hundreds of nanoseconds for $MoSe_2/WSe_2$ heterostructures [151, 160] as shown in Fig. 6(c), far surpassing lifetimes of intralayer excitons. It has been suggested that the spatial separation of the electron-hole pairs minimizes the exchange interaction that normally serves as a source of valley depolarization for excitons [149]. The long interlayer lifetimes have enabled imaging of valley-polarized exciton diffusion in a $MoSe_2/WSe_2$ heterostructure [142] and make vdW heterostructures an exciting platform for valley optoelectronic applications [57, 161]. Recent measurements of Zeeman splittings in $MoSe_2/WSe_2$ vdW heterostructures have revealed a much higher g factor of approximately 15 [141] for the interlayer exciton, which can be understood as arising from the sum of the valence and conduction valley magnetic moments.

4.2.2 Mixed layer heterostructures

Layered heterostructures provide an architecture for blending the unique properties of the constituent materials. For example, interfacing monolayer TMDs with graphene has enabled the study of novel spin physics in these hybrid systems. While graphene, with low spin-orbit coupling on the order of 10 μeV [162] and high charge conductivity, exhibits long spin diffusion lengths scales on the order of tens of micrometers at room temperature, it lacks the optical selection rules of monolayer TMDs that enable selective spin and valley excitation. In graphene/monolayer TMD vdW heterostructures, however, spin states may be optically generated in the TMD region and injected into the graphene for spin transmission as confirmed from recent spin-valve and Hanle effect measurements [163, 164].

The TMD in such a heterostructure has a proximity effect on the spin properties of graphene. Experimental and theoretical work have found that graphene inherits from the neighboring TMD a dramatic enhancement of the spin-orbit coupling reaching into the meV regime [165, 166]. The TMD also causes a reduction

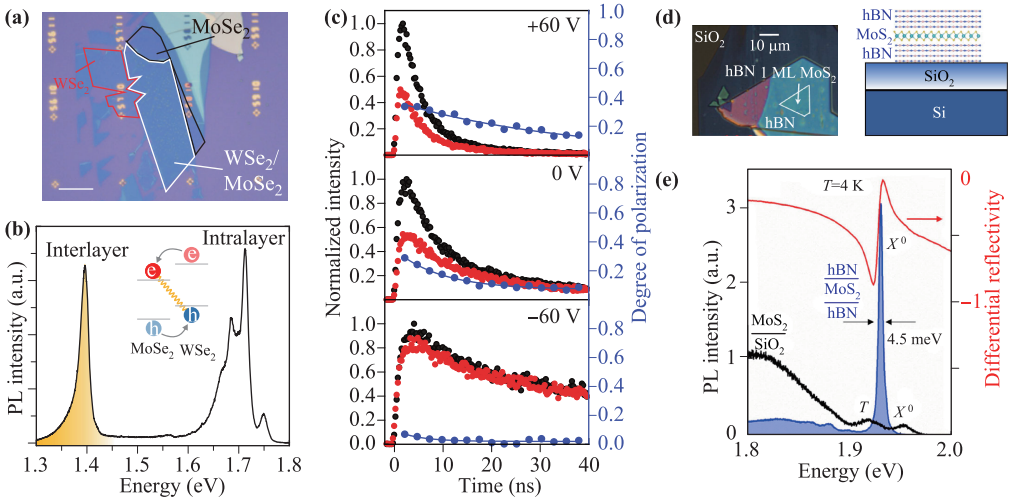

Fig. 6 Layered heterostructures of TMDs. **(a)** Optical microscope image of a monolayer $MoSe_2/WSe_2$ vdW heterostructure and **(b)** its photoluminescence spectrum at 4 K with intralayer and interlayer emission labeled. The inset illustrates the formation of the interlayer exciton via charge transfer. **(c)** Time-resolved circular photoluminescence of a $MoSe_2/WSe_2$ vdW heterostructure for σ_+ excitation with black (red) data points signifying σ_+ (σ_-) collection. Extracted valley lifetimes are 39 ± 2, 10 ± 1, and 5 ± 2 ns at gating voltages of +60, 0, and −60 V, respectively. **(d)** Optical microscope image and cartoon depiction of an encapsulated h-BN/1L-MoS_2/h-BN heterostructure. **(e)** Photoluminescence (blue) and differential reflectivity spectra of the encapsulated sample in (d) exhibiting a linewidth of 4.5 meV at 4 K for the neutral exciton. The black line shows the typical low temperature photoluminescence spectrum of a MoS_2 monolayer on a SiO_2 substrate with broader and weaker exciton peaks and a prominent lower energy defect-bound peak. Figures reproduced with permission from: (a, b) Ref. [141], Copyright © 2017 Nature Publishing Group, CC BY; (c) Ref. [142], Copyright © 2016 American Association for the Advancement of Science; (d, e) Ref. [143], Copyright © 2017 American Physical Society, licensed under CC BY.

in spin lifetimes in the graphene to the picosecond regime [167] that is highly anisotropic with about an order of magnitude difference between in-plane and out-of-plane spin states [168–170]. The spin lifetime reduction is gate-tunable [171], enabling the creation of hybrid graphene/TMD spin logic devices such as spin field-effect switches [172, 173].

4.2.3 Optimizing substrates: Hexagonal boron nitride

The substrate plays a major role in the optical and electronic response of vdW materials [174, 175]. For SiO_2 substrates grown with thermal oxidation, the rough surface leads to localized effects and strain in monolayer TMDs. When a smooth buffer is introduced, the monolayer is isolated from roughness and strain is reduced, preserving intrinsic optoelectronic properties and improving spatial homogeneity. The layered insulator hexagonal boron nitride, unlike SiO_2, is atomically flat with virtually no dangling bonds [176]. h-BN can dramatically improve the quantum yield of monolayer TMDs [8]. Since it is also a vdW material, h-BN can be easily integrated into layered material devices.

WSe_2/hBN/SiO_2 heterostructures have been used to study exciton-phonon coupling and the sensitivity of excitons to their phononic environments [177]. By adding another h-BN layer on top to form a vdW heterostructure h-BN/1L-TMD/h-BN, illustrated in Fig. 6(d), the protective h-BN can be further exploited [178]. While the bottom layer isolates the TMD from the defects of the substrate, the top encapsulating layer protects the monolayer from adsorbates and other contaminants on its surface. Encapsulated heterostructures exhibit narrower emission linewidths down to 2 meV [103, 179] for monolayer MoS_2, an order of magnitude improvement from unencapsulated monolayers [180] [Fig. 6]. Photoluminescence spectra of encapsulated layers also show a reduction of the trion [103] and localized exciton states [181]. Encapsulation has also enabled observation of photoluminescence from the 2 s excited exciton state in WSe_2 [182]. The quality and uniformity of hBN-encapsulated TMDs has been leveraged to realize quantum transport via local gates, as well as confinement of electrons and control over charged excitons at localized confinement potentials [183].

4.3 Strain engineering

Strain engineering allows manipulation of a semiconductor's optoelectronic properties through deformations of

the lattice. For monolayer TMDs, strain plays a multifaceted role in the optical response and a few key findings will be discussed here. In-plane uniaxial strain, typically achieved with a flexible polymer substrate, has been found to enable bandgap tuning of monolayer TMDs, with measurements on MoS_2 and WSe_2 demonstrating a luminescence peak shift and intensity decrease [184, 185]. This is understood as a strain-induced transition of the monolayer from a direct-bandgap semiconductor to an indirect one. Conversely, measurements on multilayer TMDs have shown an opposite effect with a transition to a direct bandgap possible [184, 185].

The application of in-plane uniaxial strain can also cause novel magnetic phenomena when the three-fold rotational symmetry of the lattice is broken. Strain can induce valley-dependent shifts between the band centers and the extrema of the magnetic moment distribution [186]. Consequently, a current applied transverse to the induced piezoelectric field results in a net magnetization of the monolayer without valley polarization. Known as the valley magnetoelectric effect, this strain-enabled magnetization has been recently observed in monolayer MoS_2 up to room temperature through spatially-resolved Kerr rotation [108].

Local strain engineering has been employed to control single photon emission in monolayer and bilayer WSe_2.

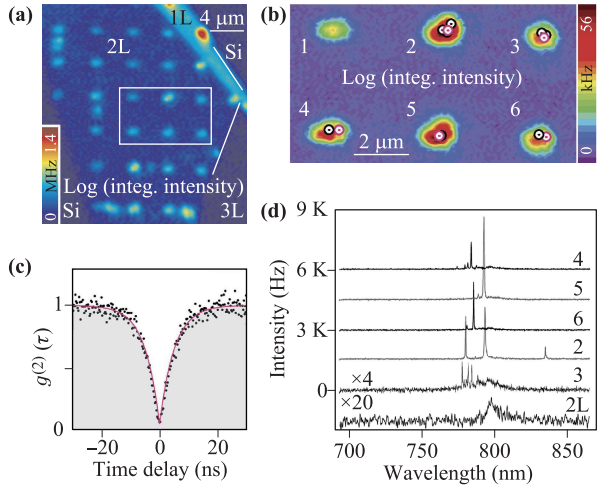

Fig. 7 Strain engineering. **(a)** Microscope image of a bilayer WSe_2 flake transferred onto an array of dielectric nanopillars overlaid with the photoluminescence integrated intensity from 700 to 860 nm. **(b)** Higher resolution spatial map covering the six nanopillars outlined in (a). **(c)** Photon auto-correlation histogram of emission from nanopillar #1 yielding $g^{(2)}(0) = 0.03 \pm 0.02$ and $\tau = 4.8 \pm 0.1$ ns. **(d)** Photoluminescence spectra of the nanopillar sites marked by a red circle contrasted with that of the bare bilayer region. Figure reproduced with permission from Ref. [187], Copyright © 2017 Nature Publishing Group, licensed under CC BY.

Localized excitons in monolayer TMDs were first found to arise from defects such as wrinkles on flat substrates. Observable at cryogenic temperatures [Fig. 7(a)], emission from these states is at lower energy than the neutral exciton, exhibits narrower linewidths (on the order of 100 μeV), has a longer lifetime, and typically appears in doublets with opposite linear polarizations, suggesting a mixing of the two valley-polarized states [30, 31, 33, 188]. Measurements of photon antibunching [Fig. 7(c)], reveal that these localized states function as single-photon emitters, making them appealing for applications in quantum optics. To this end, research has focused on the deterministic engineering of emitter states using dielectric substrates with patterned nanostructures to controllably induce local strain [32, 187, 189, 190], as shown in Fig. 7(a-b), and the fabrication of optoelectronic devices allowing electrical pumping of quantum emitters [191, 192].

In addition to mechanical applications of strain, all-optical methods have recently enabled strain engineering of TMDs via modification of the vdW interactions between layers [193]. With large photoexcited exciton population in a layer, the modified polarizability results in a local vertical compressive strain. This optically induced strain opens a new avenue for novel optomechanical devices that couple strong optical fields to high compressive forces.

4.4 Exciton confinement in monolayer nanostructures

Size-dependent features of nanostructures are common tools for manipulating properties of semiconductors, enabling tailoring of optical transitions [194, 195], magnetism [196–200], and high-mobility electronic states [201–203]. In the two-dimensional monolayer TMDs, carrier wavefunctions are naturally strongly confined in the vertical direction. Using three-dimensional confinement for size-dependent control could be useful for light emitting devices [204], energy harvesting [205], and medical sensing [206] applications, but this is challenging in the monolayer TMDs because of the small exciton Bohr radius in these materials. Despite this challenge, there has been a large body of theoretical work on the optoelectronic properties of TMDs in confined carrier regimes such as quantum dots, nanoflakes, or nanoribbons focusing on both modified electronic states and novel edge effects such as Majorana fermions [207–213].

The experimental picture has not yet caught up to the theoretical activity because of the challenge of controlling monolayers at the few nanometer size scale. MoS_2 nanotubes were investigated before the discovery of graphene [214, 215], but newer advances in lateral confinement of monolayer nanostructures have been under investigation more recently. Some of the many approaches for fabricating monolayer nanostructures in-

clude chemical exfoliation [216–219], direct growth [220], and top-down nanolithography [221]. Using chemical methods, small monolayer quantum dots can be achieved with large excitonic energy shifts [218, 219]. Electron beam patterning can create monolayer nanodots and nanoribbons with controllable size and location useful for device integration [221, 222]. Although these nanostructures preserve the valley pseudospin, the exciton confinement is still in the weak regime where intervalley mixing at edges is not significant and interesting spin-valley properties are not yet expected [223]. In contrast to these nanostructures, excitons trapped at defects in continuous monolayers can exhibit single photon emission, potentially useful for quantum emitters [30, 31, 33, 187, 188]. While these approaches to monolayer nanostructures have not yet been interfaced with monolayer photonics [224], achieving smaller laterally-confined size with better precision and repeatability are some of the current challenges for integrating monolayer nanostructures into hybrid monolayer optoelectronics.

5 Engineering optical environments in TMD optoelectronics

Complementing engineering of TMD optoelectronics by chemical and material means, there has been growing interest in controlling optoelectronic properties directly using light. This field has experienced rapid development with opportunities to explore newly discovered optical effects including coherent optical interactions [229], intervalley coherence [10], and a variety of hybrid light-matter states [40, 226]. In this section we highlight recent progress in using photonic structures, plasmonics, and high-intensity optical fields to engineer the optical environment of TMDs.

5.1 Photonic engineering

Compared to the canonical III-V semiconductors used in optoelectronic devices such as photodetectors and light-emitting diodes, the quantum yield of bare TMDs is around an order of magnitude weaker [9, 60, 227–230]. Interfacing TMDs with photonic structures can enhance their interaction with light. The atomic-scale thickness of TMDs allows for simple placement in peak evanescent fields, making them ideal candidates for integration into photonic structures.

5.1.1 Purcell effects in monolayer TMDs

The Purcell effect in exfoliated monolayer TMDs was first demonstrated by Gan *et al.* [231] in micro-photoluminescence after transfer to planar photonic crystals (PPC). The PPC had a linear three-missing hole defect with resonant modes within the monolayer MoS_2 PL spectrum. A clear enhancement of PL emission can be seen in Fig. 8(a) between the regions on the defect (region 1), off the defect but on the air holes (region 2), and off the holes (region 4). Two factors contributed to this enhancement. First, the inhibition of emission along the in-plane direction due to the presence of the in-plane bandgap, which re-directed the emission in the out-of-plane direction. This resulted in the slight enhancement of region 2 compared to region 4. Second, the Purcell effect from the cavity mode led to an enhancement of spontaneous emission by a factor of ~70 when the on and off resonance modes in region 1 were compared. This enhancement originates from the increased photon density of states and is quantified by the Purcell factor, $F_p = (3/4\pi^2)(\lambda_c/n)^3(Q/V_m)$ where λ_c, Q, and V_m are the resonant wavelength, the quality factor, and the effective mode volume of the cavity. The Purcell effect has been harnessed in monolayer TMDs interfaced with various optical cavities including PPCs [232], open cavities [233] [Fig. 8(b, c)], PPCs with rods [234], microdisks [235, 236], and ladder-type photonic crystals [237].

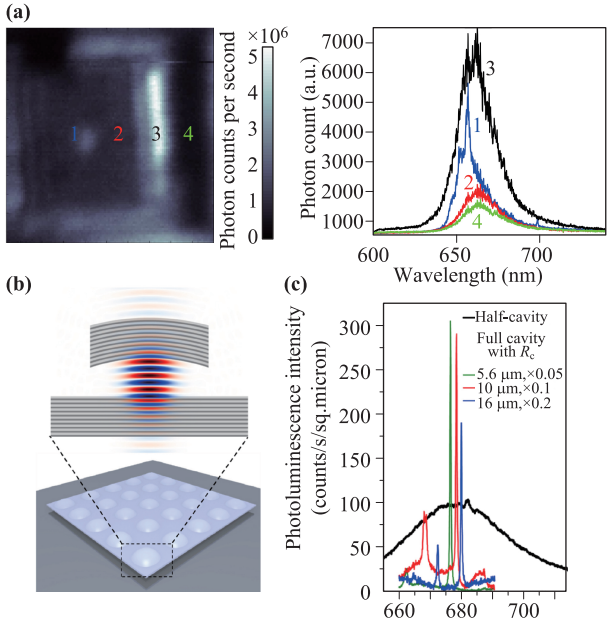

Fig. 8 Evidence of Purcell effect. **(a)** (Left) Micro-PL image showing the four different regions on the PPC. (Right) Spectra from the four regions in (a). **(b)** Schematic of an open tunable cavity formed by planar and concave Bragg reflectors. **(c)** Spectra of bare monolayer MoS_2 (black) and the cavity emission for top mirror with different radii of curvature. Figures reproduced with permission from: (a) Ref. [231], Copyright © 2013 American Institute of Physics, licensed under CC BY; (b, c) Ref. [233], Copyright © 2014 American Chemical Society, licensed under CC BY.

5.1.2 Cavity-enhanced nonlinear optics

The enhanced light-matter interaction provided by optical nanostructures also allows new opportunities to study nonlinear optical phenomena in TMD monolayers [238, 239]. While these phenomena typically require high-power optical pumping, optical microcavities can lower the power threshold to achieve second and third order nonlinearity in a material by factors of V/Q^2 and V/Q^3 respectively [240]. Cavity-enhancement of second order nonlinearity ($\chi^{(2)}$) in TMD monolayers is of particular interest due to the relative rarity of second order effects, which only occur in non-centrosymmetric crystals [241]. Such cavity-enhanced effects have been achieved using single mode cavities like photonic crystals [242] and DBR cavities [243] resonant with the pump laser, as evidenced by enhanced signals from second harmonic generation (SHG). Enhancement of SHG signals can be further increased by using double mode cavities resonant at both the pump laser and second harmonic frequencies such as using tunable Fabry–Perot cavities [244] and photonic waveguides [245]. Although this field is still nascent, realization of cavity-enhanced nonlinear effects opens up opportunities for future low-power and on-chip nonlinear devices such as frequency converters, parametric oscillators, and sensors.

5.1.3 Low-threshold lasing

An on-chip coherent light source is an essential ingredient for optoelectronic devices relevant to optical communication or computing [239–241]. Building on the foundation of enhanced luminescence, but exploiting quality factors an order of magnitude greater, low-threshold lasing at cryogenic and room temperatures has been achieved in monolayer TMDs on microdisks [49, 242], PPCs [238, 243], nanobeam cavities [244], and vertical Bragg reflector cavities [50]. Wu *et al.* [238] demonstrated the first lasing at 80 K with a WSe_2-PPC nanocavity structure [Fig. 9(a)]. Using a PPC structure similar to the one in their previous work [232], they adopted a thinner GaP top layer on PPC which led to an increase of Q from $\sim$ 200 to over 2500 due to the improved verticality of the sidewalls and a better thickness-to-lattice-constant ratio. An ultra-low lasing threshold of $\sim$ 1 W/cm^2 was achieved with continuous-wave (CW) pumping evidenced by the nonlinear "kink" in the output power dependence and the narrowing of the cavity linewidths. The β-factor, which characterizes the efficiency of spontaneous emission into the cavity mode ($\beta = 1$ means thresholdless lasing), is 0.19 [Fig. 9(b)], comparable to the value in previous quantum-dot-PPC systems [245].

Another cryogenic-temperature monolayer laser was achieved with microdisk resonators [49] [Fig. 9(c)]. Embedding WS_2 in between Si_3N_4 and hydrogen silsesquioxane to enhance mode overlap and protect the material, a high quality whispering gallery mode was achieved with cavity $Q \sim 2600$ [Fig. 9(d, e)]. The lasing threshold was met using an ultrafast pulsed pump intensity 5–8 MW/cm^2 at 10 K with $\beta = 0.5$.

More recently, lasing from monolayer TMDs at room temperature has also been achieved [50, 242–244]. Utilizing 4-layer MoS_2 sandwiched between a microdisk and a microsphere resulted in photonic $Q \sim 2500$, and lasing was attained at $\beta = 0.69$ and CW pumping > 1 kW/cm^2 [242]. In the visible spectrum, Shang *et al.* [50] created a CW vertical-cavity surface-emitting laser consisting of monolayer WS_2 sandwiched between two distributed Bragg reflectors (DBRs) of alternating layers of SiO_2 and TiO_2. For a Q-factor of about 600 after the transfer of monolayers, the lasing was achieved at a comparatively low threshold of 0.44 W/cm^2 and a high $\beta \sim 0.77$.

Because silicon is the main substrate of commercial optoelectronics, it is beneficial to have on-chip lasers operating in the infrared regime where silicon is transparent. Harnessing the emission peak energy of 1.1 eV for $MoTe_2$, Li *et al.* [244] fabricated the first infrared CW TMD laser at room temperature by improving the Q-factor to $\sim$ 5600 with their one-dimensional silicon-based photonic crystal nanobeam cavity. Both the first ($\sim$ 1050 nm) and second ($\sim$ 1130 nm) modes exhibit lasing. The lasing threshold for this laser is 6.6 W/cm^2 with $\beta = 0.1$. A recent infrared laser has been achieved using 5-layer $MoTe_2$ on PPC with longer lasing wavelength at 1305 nm [243].

5.1.4 Strong light-matter coupling: Exciton-polaritons

Although a high Q photonic structure can enhance or inhibit emission through the Purcell effect, when the photon interaction strength (typically labelled g in cavity quantum electrodynamics literature) becomes greater than the decay rates the light-matter system can enter the strong coupling regime. This regime is characterized by the creation of hybrid superpositions of light and matter states known as "polaritons" [39, 40]. Quasiparticles like plasmon-polaritons, phonon-polaritons, magnon-polaritons, and exciton-polaritons can all be created by the variety of matter states from light excitation. Here, we focus on the exciton-polaritons originating from the strong coupling between excitons in monolayer TMDs and optical photons.

Since the observation of strongly-coupled exciton-polaritons in quantum wells (QWs) [246, 247], these quasiparticles have been useful for solid state many-body physics. Although there are many realizations now, the traditional semiconductor exciton-polaritons are created when active media such as QWs are embedded in be-

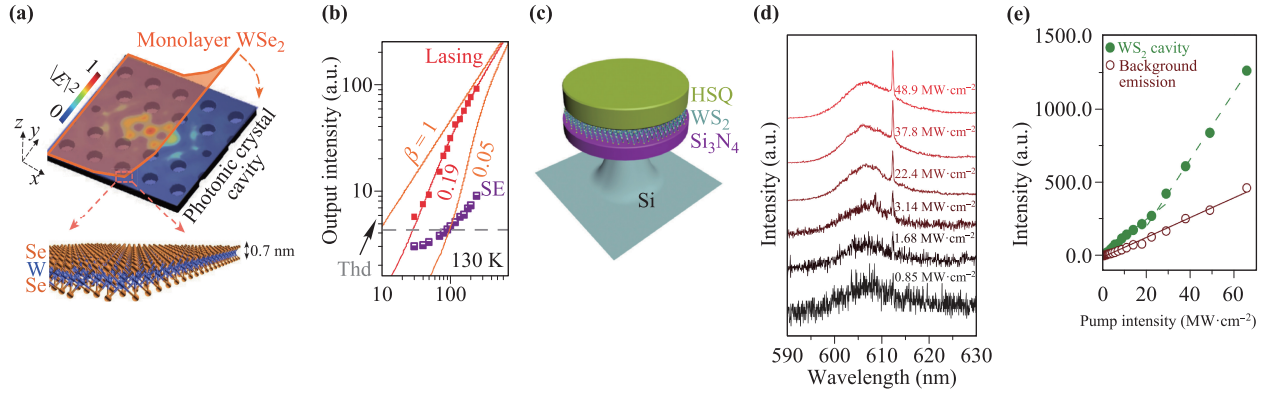

Fig. 9 Demonstration of lasing. **(a)** Schematic of monolayer WSe_2 on top of a PPC. **(b)** Output intensity versus pump power at 130 K. Cavity emission is denoted as the red-filled squares and the spontaneous emission (SE) corresponds to the purple half-filled squares. Orange lines are the simulated curves for different β-factors where $\beta = 0.19$ is the best fit to the experimental data. Grey dashed line denotes the lasing threshold. **(c)** Schematic of a monolayer WS_2 microdisk resonator. **(d)** Emission spectra showing the transition from spontaneous emission to lasing with increasing pump intensity. **(e)** Increasing pump intensity shows that only the whispering gallery mode (WGM) at 612.2 nm has lasing (green dots), evidenced by superlinear behavior. Background emission shows a regular linear relation. Figures reproduced with permission from: (a, b) Ref. [238]; (c–e) Ref. [49], Copyright © 2015 Nature Publishing Group.

tween two DBRs in a planar microcavity (MC). The DBR mirrors decrease the optical mode volume and increase the cavity electric field at the center. The resulting polariton energy eigenstates are photon "dressed states" characterized by an anticrossing energy dispersion. These light-matter polariton quasiparticles are crucial to excitonic Bose–Einstein condensation at cryogenic [248–251] or room temperature [252–256].

Strongly-coupled exciton-polaritons have been studied exhaustively in III-V and II-VI semiconductors such as GaAs and CdTe at cryogenic temperatures. In order to transition to room temperature, organic semiconductors [254] and wide bandgap semiconductors such as GaN and ZnO [252, 257, 258] have been adopted. Monolayer TMDs are also suitable for room-temperature exciton-polaritons because of their tightly-bound excitons. This feature coupled with the valley pseudospin have made monolayer TMDs attractive for novel room temperature polaritonics [259–261].

The first evidence of TMD exciton-polaritons was demonstrated by Liu *et al.* [41] in 2014 [Fig. 10(a)]. The planar MC structure consists of two DBRs each made of ∼ 8-pairs of alternating dielectric SiO_2 and Si_3N_4 layers using plasma-enhanced chemical vapor deposition (PECVD), achieving Q-factors of ∼ 100. Monolayer MoS_2, grown by chemical vapor deposition (CVD), was transferred onto the bottom DBRs before the top DBRs were grown. The MC device was studied through angle-resolved reflectivity and PL measurements where the feature of exciton-polaritons was revealed in the corresponding spectra as two dips/peaks, signifying the hybridization of light-matter states. Tracing the energy of the upper (UP) and lower (LP) polaritons, the anticrossing signature of strong coupling was observed with a Rabi splitting of 46 meV and a corresponding $g \sim 25$ meV for the MoS_2 exciton-polaritons.

In addition to MoS_2 [41, 42], other TMD materials including $MoSe_2$ [37, 262–264], WS_2 [265–270], and WSe_2 [35, 270] have also been studied with similar or modified MC structures. Dufferwiel *et al.* [262] adopted an open tunable cavity structure where precise energy detuning between the cavity photons and excitons can be achieved by adjusting the cavity length with a piezo [Fig. 10(b)]. Similar cavity tuning was also exploited by Sidler *et al.* [263] where the top DBR was on a movable fiber tip and by Flatten *et al.* [265, 266] where the top DBR was replaced by a metal film on a glass substrate. These open-cavity structures simplify tunability and electrical integration inside the MC. The hybrid metal-dielectric cavities [35, 37, 269] can also support highly localized Tamm-plasmon mode exciton-polaritons for greater vacuum field strength [271, 272]. Lastly, the photonic-crystal sub-wavelength cavities from Zhang *et al.* [270] were intended to solve the problem of high loss in the metal cavities [273] but still maintain good confinement of the optical field [274]. The structure supports polariton lasing with excellent coherence properties in GaAs QWs [275, 276].

5.1.5 *Valley-polarized exciton-polaritons*

The demonstrations of lasing and strongly coupled exciton-polaritons at room temperature due to the strong exciton binding energies in monolayer TMDs sug-

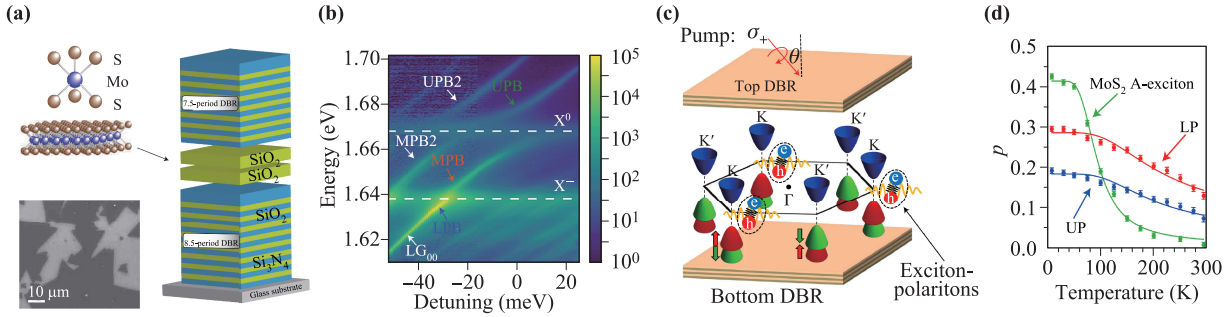

Fig. 10 Realization of monolayer TMD exciton-polaritons with valley pseudospin properties. **(a)** Schematic of a planar optical microcavity with embedded monolayer MoS_2 between two DBRs. **(b)** Emission intensity as function of energy and exciton-photon detuning. Strong coupling between cavity photons with excitons (X^0) and trions (X^-) are evidenced by anticrossings in the upper, middle, and lower polariton branches. **(c)** Schematic of valley-polarized exciton-polaritons in a TMD embedded in a microcavity. **(d)** Temperature-dependent valley polarization of bare MoS_2 A-exciton and corresponding exciton-polaritons. While the A-exciton has negligible polarization at room temperature, the UP and LP preserve the polarization. Figures reproduced with permission from (a) Ref. [41], Copyright © 2015 Nature Publishing Group; (b) Ref. [264]; (c, d) Ref. [42], Copyright © 2017 Nature Publishing Group, licensed under CC BY.

gest the utility of these layered materials for future photonic and polaritonic devices. However, what differentiates monolayer TMDs from the typical direct band gap semiconductors is the intrinsic broken symmetry in the crystals that leads to spin-valley locking [68, 70]. The valley excitons [56] in these materials are degenerate in energy but well-separated in momentum space. Although valley polarized optical emission has been reported at room temperature [83, 86, 277, 278], high valley polarization is much easier to achieve at cryogenic temperatures. Appreciable valley polarization at room temperature easily accessible for applications remains an important challenge to overcome.

A promising solution to this problem emerged from TMD exciton-poalritons, which were reported to exhibit substantial valley polarization in 2017 [42, 264, 267, 269]. In Chen *et al.* [42], valley-polarized exciton-polaritons were achieved in a planar MC with monolayer MoS_2 embedded between two DBRs [Fig. 10(c)]. Comparison of the temperature-dependent behavior of valley polarization in bare monolayer MoS_2 and MoS_2 embedded in a MC shows the stark impact of the MC on valley dynamics [Fig. 10(d)]. Utilizing the same non-resonant excitation energy, significant enhancement of valley polarization was observed from nearly zero in bare MoS_2 to of 7.5 and 13% for the MoS_2 UP and LP, respectively [Fig. 10(d)]. This significant difference was well described through a valley-specific cavity QED model including the mechanisms of coherent exciton-photon coupling, incoherent pumping, incoherent valley relaxation, and dissipation. The qualitative description is that the polariton has enhanced decay in both cavity and exciton channels, whereas intervalley scattering only impacts the excitonic part of the combined wavefunction. This picture persists in the high cooperativity regime, although in principle the model extends to more general cavity conditions. Dufferwiel *et al.* [264] demonstrated that at 4.2 K the valley polarization of exciton- and trion-polaritons in monolayer $MoSe_2$ can reach up to $\sim$ 15% compared to the vanishing polarization for the bare exciton and trion emission at the same temperature. Achieved with non-resonant excitation on their previous open tunable cavity design [262], they explain their observations by depolarization of the Coulomb exchange interaction and the Maialle–Silva–Sham (MSS) mechanism [279]. When hot excitons are created and scattered to high in-plane $\boldsymbol{k}$-vector states, the Coulomb exchange interaction leads to the longitudinal (L) and transverse (T) splitting of exciton states which disrupts the original eigenstates and gives rise to pseudospin precession. When combined with the momentum scattering by crystal disorders, this MSS mechanism leads to valley depolarization. The high efficiency of disorder scattering in bare monolayer $MoSe_2$ was reduced as exciton-polaritons have much larger spatial wavefunction than the disorder size scale, leading to a longer valley relaxation time and higher polarization. The detuning dependence was also studied showing that maximum polarization is observed when excitons and photons are on resonance, achieving a balance between relaxation to the polariton branches and radiative decay.

Instead of using non-resonant excitation, Sun *et al.* [267] used resonant pumping with planar metal cavities coated with silver to study the valley polarization of the LP branch in monolayer WS_2. At room temperature, between 12% and 27% valley polarization was observed depending on the cavity detuning. Analyzing valley pseudospin time evolution using the Liouville-von

Neumann equation, they conclude the photonic component plays the major role in depolarization in the MSS mechanism due to the metal cavities which created larger transverse electric and transverse magnetic mode splitting than the L-T splitting. The detuning dependence showed that a greater exciton portion in the polaritons leads to a longer coherence time with higher valley polarized emission observed.

A later experiment by Lundt *et al.* [269] probed the valley polarization of WS_2 polaritons in a Tamm-plasmon structure. Pumped by non-resonant light with valley polarization up to $\sim 15\%$, their work drew similar conclusions as Sun *et al.* but also shed more light on the relaxation dynamics of the polaritons and the impact of valley polarization from the dark state which is crucial in tungsten-based TMDs. Relaxation dynamics of the polaritons were investigated using a time-resolved streak-camera which showed that slower relaxation happened around energies resonant with the trion and the dark state. The coupling to the dark state at large momentum $\boldsymbol{k}$, which is believed to maintain valley polarization, causes significant preservation of polariton polarization when the bright state is nearly unpolarized. The transfer from the dark to bright state, together with acoustic phonon-assisted energy relaxation and the MSS mechanism allowed them to develop a kinetic model that reproduced the in-plane $\boldsymbol{k}$-dependence of the valley polarization. These recent studies exemplify how the valley pseudospin dynamics are modified from bare monolayer valley optoelectronics, opening a new field for exploiting photonic engineering.

5.2 Plasmonic engineering

An alternative way to control light-matter interaction is with plasmonic nanostructures. Harnessing the localized surface plasmon or surface plasmon-polariton modes at the metal/dielectric interface allows light to be confined to sub-wavelength scales. Plasmonic nanocavities based on noble metals such as gold and silver have been utilized for enhanced interaction [5, 283–285], nonlinear and ultrafast optical phenomena [286–289], antenna radiation [290–292], and surface-enhanced Raman scattering [293–295]. For monolayer TMDs, in order to im-

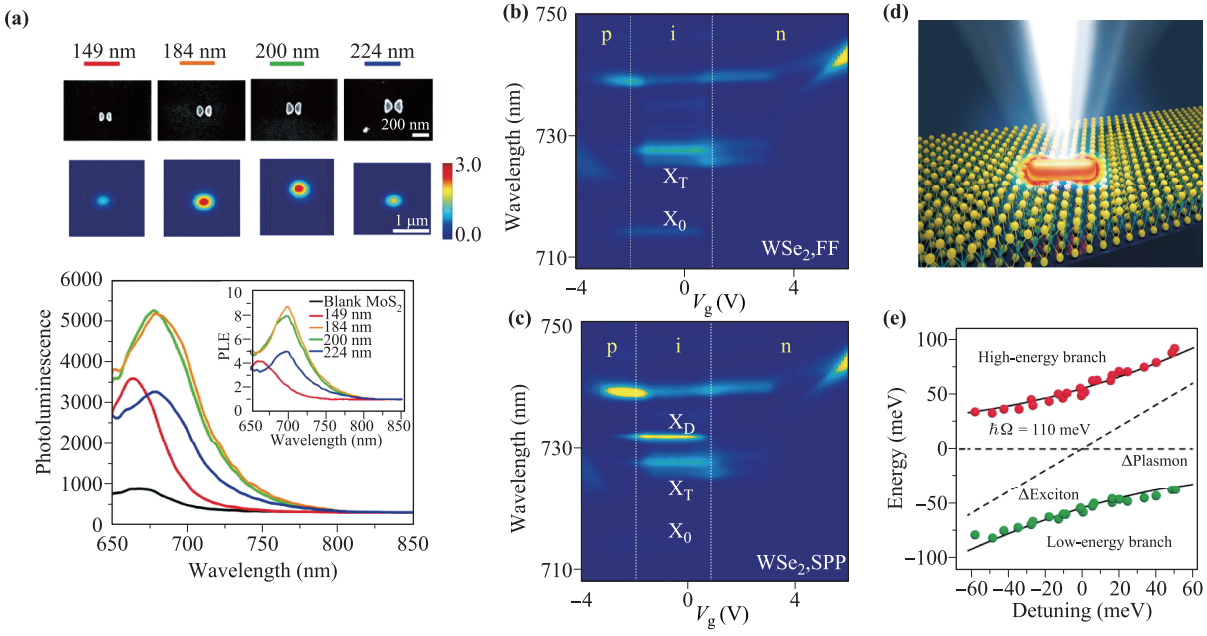

Fig. 11 Coupling of monolayer TMDs with plasmonic nanostructures. **(a)** From top to bottom: SEM images of plasmonic bowtie structures with different total lengths. Integrated emission on the corresponding structures. PL spectra taken from the locations of largest PL enhancement. (Inset) PL spectra taken from each bowtie antenna. **(b)** Far-field gate-dependent PL spectra of WSe_2. X_0 and X_T label the neutral exciton and the charged exciton emission. **(c)** Surface-plasmon-polariton (SPP) coupled PL spectra. Additional dark state (X_D) emission was seen. **(d)** Schematic of a single gold nanorod coupled to monolayer WS_2. **(e)** Anticrossing energy dispersion of the high- and low-energy branches from the scattering spectra demonstrating strong coupling between the excitons and plamons with Rabi splitting = 110 meV. Individual exciton and plasmon energies as function of detuning are shown as black dashed lines. Figures reproduced with permission from: (a) Ref. [280], Copyright © 2017 American Institute of Physics; (b, c) Ref. [281], Copyright © 2017 Nature Publishing Group; (d, e) Ref. [282], Copyright 2017 American Chemical Society.

prove their low absorption and emission efficiency, various metal plasmonic nanostructures have been adopted to increase the Purcell effect with localized gap plasmonic modes [Fig. 11(a)] such as single nanostructures [280, 296, 297], nanoparticles/disks/cubes [298–301], nanostructures in array [26, 302, 303], spiral metastructures [304], and metal-insulator interfaces [281, 305]. The spatial proximity between the metal and monolayer TMDs resulted in reduced mode volume and enhanced localized fields, creating opportunities for the manipulation of dark excitons [281] [Fig. 11(b, c)], defect bound states [303], and polarized emission [304]. However, the inherent high absorption loss in these metal structures normally kept them from reaching the strong coupling regime. Very recently, with better optical confinement, structures such as plasmonic antennas/array [226, 306, 307], single metal nanostructures [282, 308–310], metal slabs [311], and metaresonators [38] made by several groups have led to strongly coupled TMD exciton-plasmon-polaritons being achieved at room temperature with Rabi splitting over 100 meV [Fig. 11(d, e)]. Exciton-plasmon-polaritons allow novel investigation of gate-tunability [282, 306], enhanced chiral coupling [38], and entanglement between emitters [307], providing an alternative approach to future room-temperature polaritonic devices.

5.3 Optical manipulation of exciton energies

Enhancement of optical fields using engineered microcavities can have profound effects on the optical properties of TMDs. However, the microcavities themselves are not necessarily required to achieve such optical effects. Fundamentally, these modifications are induced by the strong electric field, and so similar effects can be observed using intense optical fields alone. In the weak coupling regime, when the driving optical fields are far from the exciton transition resonance, the interaction of light and matter can be understood using the language of Floquet Theory [312]. In this framework the off-resonant optical field generates a series of photon-dressed states that correspond to the coherent absorption, or stimulated emission of pump photons, shown in Fig. 12. The exciton transitions are typically modeled as a two-level system, which can hybridize with the pump-induced dressed states, leading to level repulsion. The valley-dependent optical selection rules in TMDs add additional conditions on this hybridization, since valley excitons can only interact with certain photon-dressed states depending on the polarization of the optical field [313, 314]. Hence with the appropriate pump polarization, hybridization effects such as level repulsion can be isolated to excitons in one valley, while leaving excitons in the other valley unaffected.

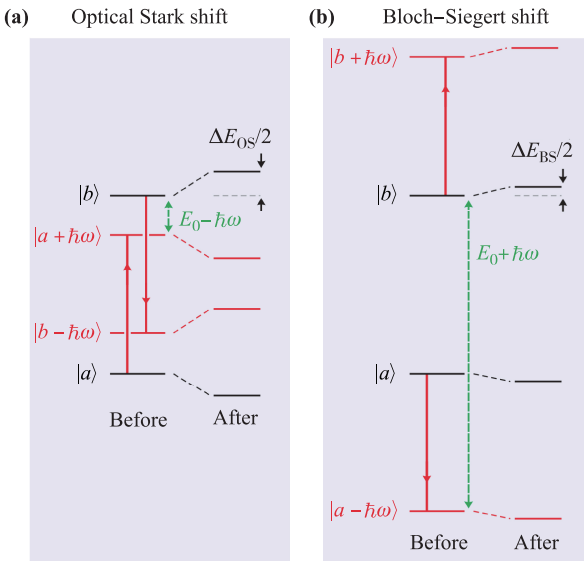

Fig. 12 Level shifts due to photon-dressed states. Schematic of **(a)** optical Stark shift ΔE_{OS} and **(b)** Bloch–Seigert shift ΔE_{BS} in a two-level system. Hybridization of exciton states with photon-dressed states leads to level repulsion. Figure reproduced with permission from Ref. [314], Copyright © 2017 American Association for the Advancement of Science.

In the simplest case of a continuous-wave pumping field, the magnitude of the energy level shift is given by

$$\Delta E_{cw} = \overbrace{\frac{1}{2}\frac{|\mathcal{M}|^2\mathcal{E}^2}{E_0 - h\nu}}^{\text{Optical Stark shift}} + \overbrace{\frac{1}{2}\frac{|\mathcal{M}|^2\mathcal{E}^2}{E_0 + h\nu}}^{\text{Bloch–Siegert shift}}, \qquad (2)$$

where $\mathcal{M}$ is the transition dipole moment of the exciton transition, $\mathcal{E}$ is the amplitude of the pump electric field, and E_0 is the unperturbed exciton transition energy. There are two terms governing the magnitude of the shift, each with a different dependence on the pump detuning from E_0. The first term, known as the optical Stark shift, dominates when $h\nu \approx E_0$ and has been observed in WS_2 [313, 314], WSe_2 [101, 225, 315], MoS_2 [315] and ReS_2 [316]. The second term, known as the Bloch–Siegert shift, only becomes significant at large pump detuning, and has recently been observed in WS_2 [314]. Since these effects are proportional to the amplitude of the electric field, most experiments investigating these level shifts in semiconductors employ pulsed lasers [101, 225, 313–320]. When ultrafast pulses are used, the continuous wave approximation from Eq. (2) is no longer accurate. However, the corrections accounting for finite optical pulses typically only influence the *magnitude* of the observed shift [315], and so the characteristic scaling with pump field intensity and detuning still persists in ultrafast measurements [314].

5.3.1 Optical Stark effect

In TMD monolayers, the optical Stark effect (OSE) can be selectively applied to a single valley by using a circularly-polarized pump [225, 313, 314]. This causes the exciton absorption resonance in one valley to blueshift, leading to a polarization-dependent change in the optical response of the material near the exciton resonance [Fig. 13(a)]. This valley-exclusive blueshift can be detected using a variety of polarization-dependent pump-probe techniques, including time-resolved reflectance [225, 313–315, 321], transmission [316], and Kerr rotation [315]. Since the Stark shift results from a coherent interaction between the pump field and the exciton states, the shift in energy only occurs during the duration of the pump pulse. Hence a characteristic feature of the optical Stark effect in all of these measurements is a signal with symmetric rise and decay dynamics that are limited by the pulsewidths used in the experiment.

The most intuitive OSE measurement occurs in the case of time-resolved reflectance and transmission measurements on transparent substrates, from which the absorbance spectrum is easily extracted [313, 316]. In these measurements the circularly-polarized pump generates a Stark shift ΔE in one valley, which induces circular birefringence ($\tilde{n}_+ \neq \tilde{n}_-$). A co-circularly polarized probe that interacts with the same valley as the pump is used to measure the change in absorbance $\Delta\alpha$ induced by the blueshift [Fig. 13(b)]. Valley-exclusivity of the Stark shift is confirmed by repeating this measurement with an oppositely circularly-polarized probe. In this case, the pump and probe interact with opposite valleys, and so no change in absorption is detected by the probe [Fig. 13(c)]. In the case of reflective substrates, the relationship between reflectance, transmittance, and absorbance becomes more complicated, but a similar analysis can be performed using the imaginary part of the TMD refractive index in lieu of the absorbance spectrum [101, 315].

The pump-induced circular birefringence can also be detected by the Kerr rotation angle θ of linearly polarized light reflected off the material, which provides an additional method for measuring this effect [315] [Fig. 13(d)]. While reflectance and transmission measurements probe the change in absorption in one valley, Kerr rotation measures the phase difference between the components of circular polarization induced by the OSE. Kerr rotation has the advantage of automatically rejecting any polarization-independent background signals, which can significantly increase the measurement's sensitivity to the OSE signal by suppressing background noise [315]. However, since Kerr rotation directly measures the *difference* between the optical response at the two valleys, it cannot be used to single out pump-induced changes

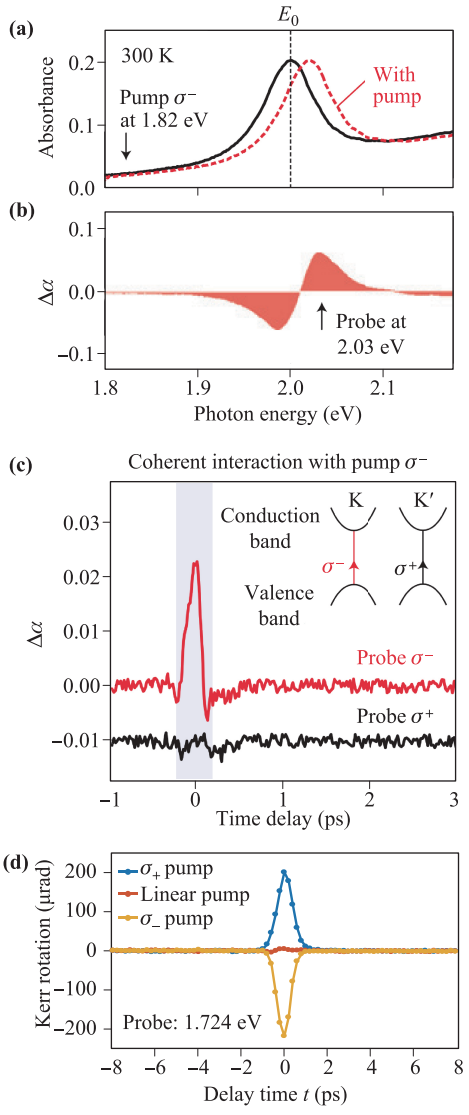

Fig. 13 Pump-probe measurements of the valley-selective optical Stark effect. **(a)** Blueshift in exciton absorption resonance caused by a subresonant circularly-polarized pump pulse. **(b)** Differential absorption signal induced by the blueshift shown in (a). **(c)** Stark shift measured by time-resolved reflectance for σ_- pump, showing probe polarization dependence. **(d)** Stark shift measured by time-resolved Kerr rotation. Probe is linearly polarized. The direction of rotation induced by the pump changes sign with pump polarization. Figures reproduced with permission from: (a–c) Ref. [313], Copyright © 2015 Nature Publishing Group; (d) Ref. [315], Copyright © 2017 American Physical Society.

in an individual valley. The ability to address each valley individually is important for measurements of more complicated valley optical stark effects such as the biexcitonic optical Stark effect [322] and the Bloch–Siegert shift [314], which cause pump-induced shifts at both valleys that need to be measured independently (Section

5.3.3). For these measurements, Kerr rotation may be inadequate.

5.3.2 All-optical coherent valley manipulation

The valley-selective optical Stark effect generates an effective magnetic field that lifts the valley degeneracy in TMDs, and can therefore be used for quantum coherent control of the valley pseudospin [101]. This approach follows from extensive use of the optical Stark effect for quantum manipulation of spin-based qubits [323–328], where the subresonant "tipping pulse" breaks spin degeneracy, which induces a phase difference between the two spin states that corresponds to a coherent rotation of spin [324]. The physics are analogous for valley pseudospin, and the induced rotation is proportional to both the intensity and duration of the tipping pulse [101]. These optical pulses provide access to ultrafast timescales, which allows for a direct investigation of the dynamics of valley coherence [101] as opposed to the steady-state phenomena probed by DC magnetic fields [100, 102]. Moreover, a valley-based implementation of quantum computation will require multiple operations on a coherent valley state before the system decoheres [329], which can be provided by ultrafast pulses [324].

In the work by Ye *et al.*, valley coherence in WSe_2 is monitored using a slight variation of the standard linearly-polarized photoluminescence measurement discussed in Section 3.2.1. In the absence of a tipping pulse, a linearly polarized excitation pulse generates a superposition of the two degenerate valley exciton states [Fig. 14(a)]. Pseudospin rotation is achieved by exciting a superposition of valley states, and then immediately breaking the valley degeneracy with a tipping pulse. The tipping pulse must be applied within the valley coherence time of the superposition in order to produce a rotation of the linearly-polarized PL [Fig. 14(b)]. If the tipping pulse is applied after the excited state decoheres, the PL will be co-polarized with the excitation pulse. This provides a means of probing the valley decoherence time by measuring the PL rotation as a function of the delay between the excitation tipping pulses [Fig. 14(c)]. From this measurement a valley decoherence time of $T_{valley} = 350 \pm 50$ fs is extracted [101], in good agreement with previous measurements of this quantity using different techniques [105, 330, 331].

5.3.3 Bloch–Siegert shift and biexcitonic Stark effect

When the pump energy is highly detuned from the exciton transition energy, the Bloch–Seigert shift becomes comparable in magnitude to the Stark shift [314]. Interestingly, for a given circularly-polarized pump, the optical Stark and Bloch–Siegert shifts occur in opposite valleys and can therefore be completely disentan-

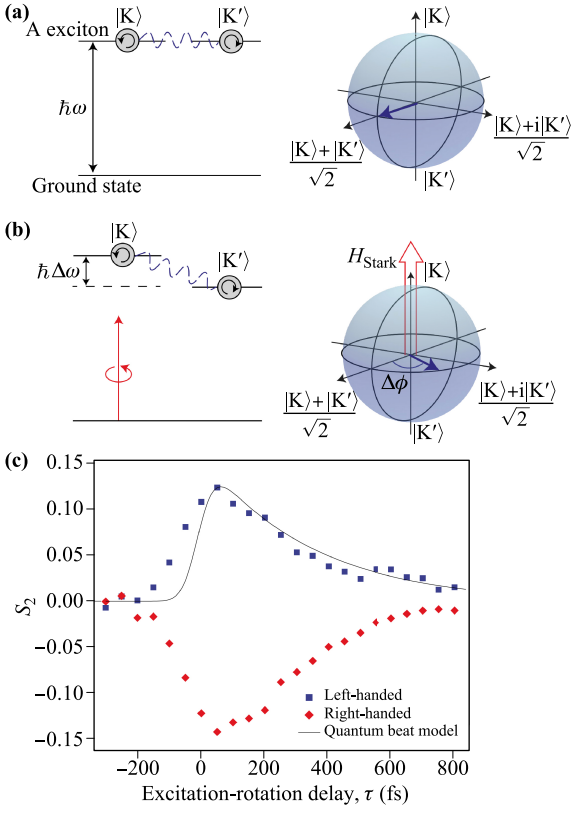

Fig. 14 Coherent optical control of valley pseudospin using optical Stark effect. **(a)** Linearly polarized pulse excites a superposition of the K and K' excitons at energy $\hbar\omega$. This corresponds to a pseudospin that lies in the equitorial plane of the Bloch sphere. **(b)** Subresonant, circularly polarized tipping pulse selectively increases the exciton transition energy at the K valley by $\hbar\Delta\omega$. While the control pulse is present, a phase difference $\Delta\phi$ accumulates between the valleys, corresponding to a rotation on the Bloch sphere. This is analogous to the rotation produced by an out-of-plane magnetic field (Open arrow). **(c)** Stokes parameter S_2 of photoluminescence as a function of excitation-rotation delay time. This measurement can be used to extract the valley coherence time. Figures reproduced with permission from Ref. [101], Copyright © 2016 Nature Publishing Group.

gled by polarization. This distinguishability is possible because the Bloch–Seigert shift is induced by the "counter-rotating" component of the pump field, which obeys the opposite polarization-dependent selection rules as the "co-rotating" component that causes the optical Stark effect.

Intervalley biexcitons provide another mechanism to optically induce level shifts in both valleys with a circularly polarized pump. Intervalley biexcitons are bound pairs of excitons from opposite valleys that obey different selection rules than the single exciton transitions, providing a channel for coupling between the pump and the opposite valley that is otherwise forbidden. This biexci-

tonic optical stark effect has been observed in WS_2 using a blue-detuned circularly polarized pump, which causes the expected energy downshift in the excitation valley and a biexciton-mediated energy upshift in the opposite valley [322].

6 Summary and outlook

Engineering the electronic and optical environment of monolayer TMDs and related van der Waals materials has made great strides in recent years. With the growing taxonomy of layered compounds and new approaches to tailor their properties, a large interdisciplinary community is fast exploring transformative applications. Since the initial discoveries of direct bandgaps in monolayer TMDs, numerous ideas and opportunities have focused on harnessing the features of these materials specifically for optoelectronics. While the bandgap makes this endeavor attractive for this particular material class, the motivation for the explosion of interest is both more complex and more subtle.

This review has highlighted some of the interesting optical features in monolayer TMDs. Although the combination of low-dimensionality, strong optical features, and spin physics that characterize much of the novel literature of TMDs is not unique, these layered materials also bring to the table the exciting potential for treating materials as building blocks with external access to the entire crystal. Many of the specific advances and interest in optoelectronic devices utilizing these materials can be framed in terms of this capability, a feature of the van der Waals materials more generally. Setting aside the obvious potential for flexible optoelectronics afforded by materials at the atomic limits of thickness, the ability to take advantage of this all-surface geometry in order to tailor the desired optoelectronic properties highlights the importance of expanding the toolbox for manipulating materials [11–14].

For TMD optoelectronics specifically, which occupied much of this review, these materials allow new avenues of manipulation in devices using valley pseudospin. As one example, spectral separation of the valley exciton peaks could be used for non-reciprocal photonic devices such as optical isolators which require breaking of time-reversal symmetry [332–334]. Typically high external magnetic fields are needed to accomplish this, but integration of monolayer TMDs with ferromagnetic substrates such as CrI_3 could allow tailored magnetic properties for such applications, for instance exchange fields of up to 13 T as achieved in a WSe_2/CrI_3 vertical heterostructure [335].

In the context of photonic engineering of TMDs, the possibilities for polaritonics have been brightening [40]. The ability to tailor TMD optical environments has opened the potential both for interesting physics such as valley-polarized polariton condensation [248], optical Hall effects [336, 337], and topological polaritonics [338, 339] as well as applications such as low-threshold monolayer polaritonic devices for optical logic [260, 340–342].

Despite the opportunities suggested here and the many more without space to mention, monolayer TMD optoelectronics faces certain challenges. Historically, other material systems have already achieved far greater sophistication and optimization; despite advances in both vapor deposition and molecular beam epitaxy of TMDs, growth is not yet as optimized as would be required for scalability. Integration of materials and devices together, either to tailor layered heterostructures [11] or to create more diverse multi-dimensional heterostructures [14] is still in its infancy. The forthcoming refinement of approaches to engineer the electronic and optical environment of layered materials promises to make these materials ever more relevant for optoelectronic applications.

Acknowledgements The authors acknowledge support by the Office of Naval Research under Grant No. N00014-16-1-3055, the U.S. Department of Energy, Office of Basic Energy Sciences, Division of Materials Sciences and Engineering under award No. DE-SC0012130, and National Science Foundation MRSEC program under grant No. DMR-1720139 at the Materials Research Center of Northwestern University.

References

1. K. Barnham and G. Duggan, A new approach to high-efficiency multi-band-gap solar cells, *J. Appl. Phys.* 67(7), 3490 (1990)
2. N. N. Ledentsov, V. M. Ustinov, V. A. Shchukin, P. S. Kop'ev, Z. I. Alferov, and D. Bimberg, Quantum dot heterostructures: Fabrication, properties, lasers, *Semiconductors* 32(4), 343 (1998)
3. C. Strümpel, M. McCann, G. Beaucarne, V. Arkhipov, A. Slaoui, V. Švrček, C. Del Canizo, and I. Tobias, Modifying the solar spectrum to enhance silicon solar cell efficiency — An overview of available materials, *Sol. Energy Mater. Sol. Cells* 91(4), 238 (2007)
4. U. K. Mishra, P. Parikh, and Y. F. Wu, AlGaN/GaN HEMTs-an overview of device operation and applications, *Proc. IEEE* 90(6), 1022 (2002)
5. H. A. Atwater and A. Polman, Plasmonics for improved photovoltaic devices, *Nat. Mater.* 9(3), 205 (2010)
6. M. N. Baibich, J. M. Broto, A. Fert, F. N. Van Dau, F. Petroff, P. Etienne, G. Creuzet, A. Friederich, and J. Chazelas, Giant magnetoresistance of (001)Fe/(001)Cr magnetic superlattices, *Phys. Rev. Lett.* 61(21), 2472 (1988)

7. S. Bader and S. Parkin, Spintronics, *Annu. Rev.: Condens. Matter Phys.* 1(1), 71 (2010)
8. K. F. Mak, K. He, J. Shan, and T. F. Heinz, Control of valley polarization in monolayer MoS_2 by optical helicity, *Nat. Nanotechnol.* 7(8), 494 (2012)
9. M. Amani, P. Taheri, R. Addou, G. H. Ahn, D. Kiriya, D. H. Lien, R. M. III Ager, Wallace, and A. Javey, Recombination kinetics and effects of superacid treatment in sulfur- and selenium-based transition metal dichalcogenides, *Nano Lett.* 16(4), 2786 (2016)
10. A. M. Jones, H. Yu, N. J. Ghimire, S. Wu, G. Aivazian, J. S. Ross, B. Zhao, J. Yan, D. G. Mandrus, D. Xiao, W. Yao, and X. Xu, Optical generation of excitonic valley coherence in monolayer WSe_2, *Nat. Nanotechnol.* 8(9), 634 (2013)
11. K. Novoselov and A. C. Neto, Two-dimensional crystals-based heterostructures: Materials with tailored properties, *Phys. Scr.* 2012, 014006 (2012)
12. A. K. Geim and I. V. Grigorieva, Van der Waals heterostructures, *Nature* 499(7459), 419 (2013)
13. K. Novoselov, A. Mishchenko, A. Carvalho, and A. C. Neto, 2D materials and van der Waals heterostructures, *Science* 353(6298), aac9439 (2016)
14. D. Jariwala, T. J. Marks, and M. C. Hersam, Mixed-dimensional van der Waals heterostructures, *Nat. Mater.* 16(2), 170 (2017)
15. B. Radisavljevic, M. B. Whitwick, and A. Kis, Integrated circuits and logic operations based on single-layer MoS_2, *ACS Nano* 5(12), 9934 (2011)
16. D. Ovchinnikov, A. Allain, Y.S. Huang, D. Dumcenco, and A. Kis, Electrical transport properties of single-layer WS_2, *ACS Nano* 8(8), 8174 (2014)
17. J. Lee, K. F. Mak, and J. Shan, Electrical control of the valley Hall effect in bilayer MoS_2 transistors, *Nat. Nanotechnol.* 11(5), 421 (2016)
18. Z. Wang, J. Shan, and K. F. Mak, Valley- and spin-polarized Landau levels in monolayer WSe_2, *Nat. Nanotechnol.* 12(2), 144 (2016)
19. D. Wu, X. Li, L. Luan, X. Wu, W. Li, M. N. Yogeesh, R. Ghosh, Z. Chu, D. Akinwande, Q. Niu, and K. Lai, Uncovering edge states and electrical inhomogeneity in MoS_2 field-effect transistors, *Proc. Natl. Acad. Sci. USA* 113(31), 8583 (2016)
20. Y. Jia, T. K. Stanev, E. J. Lenferink, and N. P. Stern, Enhanced conductivity along lateral homojunction interfaces of atomically thin semiconductors, *2D Materials* 4, 021012 (2017)
21. S. Das, H. Y. Chen, A. V. Penumatcha, and J. Appenzeller, High performance multilayer MoS_2 transistors with scandium contacts, *Nano Lett.* 13(1), 100 (2013)
22. B. Radisavljevic, M. B. Whitwick, and A. Kis, Small-signal amplifier based on single-layer MoS_2, *Appl. Phys. Lett.* 101(4), 043103 (2012)
23. J. Pu, Y. Yomogida, K. K. Liu, L. J. Li, Y. Iwasa, and T. Takenobu, Highly flexible MoS_2 thin-film transistors with ion gel dielectrics, *Nano Lett.* 12(8), 4013 (2012)
24. H.Y. Chang, S. Yang, J. Lee, L. Tao, W.S. Hwang, D. Jena, N. Lu, and D. Akinwande, High-performance, highly bendable MoS_2 transistors with high-K dielectrics for flexible low-power systems, *ACS Nano* 7, 5446 (2013)
25. K. Wang, Y. Feng, C. Chang, J. Zhan, C. Wang, Q. Zhao, J. N. Coleman, L. Zhang, W. J. Blau, and J. Wang, Broadband ultrafast nonlinear absorption and nonlinear refraction of layered molybdenum dichalcogenide semiconductors, *Nanoscale* 6(18), 10530 (2014)
26. H. Yu, D. Talukdar, W. Xu, J. B. Khurgin, and Q. Xiong, Charge-induced second-harmonic generation in bilayer WSe_2, *Nano Lett.* 15(8), 5653 (2015)
27. G. Wang, X. Marie, I. Gerber, T. Amand, D. Lagarde, L. Bouet, M. Vidal, A. Balocchi, and B. Urbaszek, Giant enhancement of the optical second-harmonic emission of WSe_2 monolayers by laser excitation at exciton resonances, *Phys. Rev. Lett.* 114(9), 097403 (2015)
28. K. L. Seyler, J. R. Schaibley, P. Gong, P. Rivera, A. M. Jones, S. Wu, J. Yan, D. G. Mandrus, W. Yao, and X. Xu, Electrical control of second-harmonic generation in a WSe_2 monolayer transistor, *Nat. Nanotechnol.* 10(5), 407 (2015)
29. Z. Sun, A. Martinez, and F. Wang, Optical modulators with 2D layered material, *Nat. Photon.* 10(4), 227 (2016)
30. Y. M. He, G. Clark, J. R. Schaibley, Y. He, M. C. Chen, Y. J. Wei, X. Ding, Q. Zhang, W. Yao, X. Xu, C.Y. Lu, and J. W. Pan, Single quantum emitters in monolayer semiconductors, *Nat. Nanotechnol.* 10(6), 497 (2015)
31. A. Branny, G. Wang, S. Kumar, C. Robert, B. Lassagne, X. Marie, B. D. Gerardot, and B. Urbaszek, Discrete quantum dot like emitters in monolayer $MoSe_2$: Spatial mapping, magneto-optics, and charge tuning, *Appl. Phys. Lett.* 108(14), 142101 (2016)
32. S. Kumar, A. Kaczmarczyk, and B. D. Gerardot, Strain-induced spatial and spectral isolation of quantum emitters in mono- and bilayer WSe_2, *Nano Lett.* 15(11), 7567 (2015)
33. A. Srivastava, M. Sidler, A. V. Allain, D. S. Lembke, A. Kis, and A. Imamoğlu, Optically active quantum dots in monolayer WSe_2, *Nat. Nanotechnol.* 10(6), 491 (2015)
34. J. Miao, W. Hu, Y. Jing, W. Luo, L. Liao, A. Pan, S. Wu, J. Cheng, X. Chen, and W. Lu, Surface plasmon-enhanced photodetection in few layer MoS_2 phototransistors with Au nanostructure arrays, *Small* 11(20), 2392 (2015)
35. N. Lundt, S. Klembt, E. Cherotchenko, S. Betzold, O. Iff, A. V. Nalitov, M. Klaas, C. P. Dietrich, A. V. Kavokin, S. Höfling, and C. Schneider, Room-temperature Tamm-plasmon exciton-polaritons with a WSe_2 monolayer, *Nat. Commun.* 7, 13328 (2016)

36. S. Butun, E. Palacios, J. D. Cain, Z. Liu, V. P. Dravid, and K. Aydin, Quantifying plasmon-enhanced light absorption in monolayer WS_2 films, *ACS Appl. Mater. Interfaces* 9(17), 15044 (2017)

37. N. Lundt, P. Nagler, A. Nalitov, S. Klembt, M. Wurdack, S. Stoll, T. Harder, S. Betzold, V. Baumann, A. Kavokin, et al., Valley polarized relaxation and upconversion luminescence from tamm-plasmon trion-polaritons with a $MoSe_2$ monolayer, *2D Materials* 4, 025096 (2017)

38. T. Chervy, S. Azzini, E. Lorchat, S. Wang, Y. Gorodetski, J. A. Hutchison, S. Berciaud, T. W. Ebbesen, and C. Genet, Room temperature chiral coupling of valley excitons with spin-momentum locked surface plasmons, *ACS Photon.* 5(4), 1281 (2018)

39. T. Low, A. Chaves, J. D. Caldwell, A. Kumar, N. X. Fang, P. Avouris, T. F. Heinz, F. Guinea, L. Martin-Moreno, and F. Koppens, Polaritons in layered two-dimensional materials, *Nat. Mater.* 16(2), 182 (2017)

40. D. N. Basov, M. M. Fogler, and F. J. Garcia de Abajo, Polaritons in van der Waals materials, *Science* 354(6309), aag1992 (2016)

41. X. Liu, T. Galfsky, Z. Sun, F. Xia, E. C. Lin, Y. H. Lee, S. Kéna-Cohen, and V. M. Menon, Strong light–matter coupling in two-dimensional atomic crystals, *Nat. Photon.* 9(1), 30 (2015)

42. Y. J. Chen, J. D. Cain, T. K. Stanev, V. P. Dravid, and N. P. Stern, Valley-polarized exciton–polaritons in a monolayer semiconductor, *Nat. Photon.* 11(7), 431 (2017)

43. J. Pak, J. Jang, K. Cho, T. Y. Kim, J. K. Kim, Y. Song, W. K. Hong, M. Min, H. Lee, and T. Lee, Enhancement of photodetection characteristics of MoS_2 field effect transistors using surface treatment with copper phthalocyanine, *Nanoscale* 7(44), 18780 (2015)

44. L. Britnell, R. Ribeiro, A. Eckmann, R. Jalil, B. Belle, A. Mishchenko, Y. J. Kim, R. Gorbachev, T. Georgiou, S. Morozov, et al., Strong light-matter interactions in heterostructures of atomically thin films, *Science* 340(6138), 1311 (2013)

45. A. Pospischil, M. M. Furchi, and T. Mueller, Solar-energy conversion and light emission in an atomic monolayer p–n diode, *Nat. Nanotechnol.* 9(4), 257 (2014)

46. F. Withers, O. Del Pozo-Zamudio, A. Mishchenko, A. Rooney, A. Gholinia, K. Watanabe, T. Taniguchi, S. Haigh, A. Geim, A. Tartakovskii, and K. S. Novoselov, Light-emitting diodes by band-structure engineering in van der Waals heterostructures, *Nat. Mater.* 14(3), 301 (2015)

47. J. S. Ross, P. Klement, A. M. Jones, N. J. Ghimire, J. Yan, D. Mandrus, T. Taniguchi, K. Watanabe, K. Kitamura, W. Yao, D. H. Cobden, and X. Xu, Electrically tunable excitonic light-emitting diodes based on monolayer WSe_2 p–n junctions, *Nat. Nanotechnol.* 9(4), 268 (2014)

48. B. W. Baugher, H. O. Churchill, Y. Yang, and P. Jarillo-Herrero, Optoelectronic devices based on electrically tunable p–n diodes in a monolayer dichalcogenide, *Nat. Nanotechnol.* 9(4), 262 (2014)

49. Y. Ye, Z. J. Wong, X. Lu, X. Ni, H. Zhu, X. Chen, Y. Wang, and X. Zhang, Monolayer excitonic laser, *Nat. Photon.* 9(11), 733 (2015)

50. J. Shang, C. Cong, Z. Wang, N. Peimyoo, L. Wu, C. Zou, Y. Chen, X. Y. Chin, J. Wang, C. Soci, W. Huang, and T. Yu, Room-temperature 2D semiconductor activated vertical-cavity surface-emitting lasers, *Nat. Commun.* 8(1), 543 (2017)

51. L. Peng, Y. Yuan, G. Li, X. Yang, J. J. Xian, C. J. Yi, Y. G. Shi, and Y. S. Fu, Observation of topological states residing at step edges of WTe_2, *Nat. Commun.* 8(1), 659 (2017)

52. I. Belopolski, D. S. Sanchez, Y. Ishida, X. Pan, P. Yu, S. Y. Xu, G. Chang, T. R. Chang, H. Zheng, N. Alidoust, et al., Discovery of a new type of topological Weyl fermion semimetal state in $Mo_xW_{1-x}Te_2$, *Nat. Commun.* 7, 13643 (2016)

53. Y. Zhang, T. Oka, R. Suzuki, J. Ye, and Y. Iwasa, Electrically switchable chiral light-emitting transistor, *Science* 344(6185), 725 (2014)

54. Q. H. Wang, K. Kalantar-Zadeh, A. Kis, J. N. Coleman, and M. S. Strano, Electronics and optoelectronics of two-dimensional transition metal dichalcogenides, *Nat. Nanotechnol.* 7(11), 699 (2012)

55. M. Chhowalla, H. S. Shin, G. Eda, L. J. Li, K. P. Loh, and H. Zhang, The chemistry of two-dimensional layered transition metal dichalcogenide nanosheets, *Nat. Chem.* 5(4), 263 (2013)

56. H. Yu, X. Cui, X. Xu, and W. Yao, Valley excitons in two-dimensional semiconductors, *Natl. Sci. Rev.* 2(1), 57 (2015)

57. J. R. Schaibley, H. Yu, G. Clark, P. Rivera, J. S. Ross, K. L. Seyler, W. Yao, and X. Xu, Valleytronics in 2D materials, *Nat. Rev. Mater.* 1(11), 16055 (2016)

58. W. T. Hsu, Y. L. Chen, C. H. Chen, P. S. Liu, T. H. Hou, L. J. Li, and W. H. Chang, Optically initialized robust valley-polarized holes in monolayer WSe_2, *Nat. Commun.* 6, 8963 (2015)

59. X. X. Zhang, T. Cao, Z. Lu, Y. C. Lin, F. Zhang, Y. Wang, Z. Li, J. C. Hone, J. A. Robinson, D. Smirnov, S. G. Louie, and T. F. Heinz, Magnetic brightening and control of dark excitons in monolayer WSe_2, *Nat. Nanotechnol.* 12(9), 883 (2017)

60. K. F. Mak, C. Lee, J. Hone, J. Shan, and T. F. Heinz, Atomically thin MoS_2: A new direct-gap semiconductor, *Phys. Rev. Lett.* 105(13), 136805 (2010)

61. T. Cheiwchanchamnangij and W. R. Lambrecht, Quasiparticle band structure calculation of monolayer, bilayer, and bulk MoS_2, *Phys. Rev. B* 85(20), 205302 (2012)

62. A. Chernikov, T. C. Berkelbach, H. M. Hill, A. Rigosi, Y. Li, O. B. Aslan, D. R. Reichman, M. S. Hybertsen, and T. F. Heinz, Exciton binding energy and nonhydrogenic Rydberg series in monolayer WS_2, *Phys. Rev. Lett.* 113(7), 076802 (2014)

63. K. F. Mak, K. He, C. Lee, G. H. Lee, J. Hone, T. F. Heinz, and J. Shan, Tightly bound trions in monolayer MoS_2, *Nat. Mater.* 12(3), 207 (2013)

64. J. Klein, J. Wierzbowski, A. Regler, J. Becker, F. Heimbach, K. Müller, M. Kaniber, and J. J. Finley, Stark effect spectroscopy of mono- and few-layer MoS_2, *Nano Lett.* 16(3), 1554 (2016)

65. K. C. Wang, T. K. Stanev, D. Valencia, J. Charles, A. Henning, V. K. Sangwan, A. Lahiri, D. Mejia, P. Sarangapani, M. Povolotskyi, et al., Control of interlayer physics in 2H transition metal dichalcogenides, *J. Appl. Phys.* 122(22), 224302 (2017)

66. Z. Wang, Y. H. Chiu, K. Honz, K. F. Mak, and J. Shan, Electrical tuning of interlayer exciton gases in WSe_2 bilayers, *Nano Lett.* 18(1), 137 (2018)

67. J. S. Ross, S. Wu, H. Yu, N. J. Ghimire, A. M. Jones, G. Aivazian, J. Yan, D. G. Mandrus, D. Xiao, W. Yao, and X. Xu, Electrical control of neutral and charged excitons in a monolayer semiconductor, *Nat. Commun.* 4, 1474 (2013)

68. D. Xiao, G. B. Liu, W. Feng, X. Xu, and W. Yao, Coupled spin and valley physics in monolayers of MoS_2 and other group-VI dichalcogenides, *Phys. Rev. Lett.* 108(19), 196802 (2012)

69. A. Kormányos, G. Burkard, M. Gmitra, J. Fabian, V. Zólyomi, N. D. Drummond, and V. Falko, $k \cdot p$ theory for two-dimensional transition metal dichalcogenide semiconductors, *2D Materials* 2, 022001 (2015)

70. X. Xu, W. Yao, D. Xiao, and T. F. Heinz, Spin and pseudospins in layered transition metal dichalcogenides, *Nat. Phys.* 10(5), 343 (2014)

71. T. Yu and M. Wu, Valley depolarization due to intervalley and intravalley electron-hole exchange interactions in monolayer MoS_2, *Phys. Rev. B* 89(20), 205303 (2014)

72. W. Yao, D. Xiao, and Q. Niu, Valley-dependent optoelectronics from inversion symmetry breaking, *Phys. Rev. B* 77(23), 235406 (2008)

73. K. F. Mak, K. L. McGill, J. Park, and P. L. McEuen, The valley Hall effect in MoS_2 transistors, *Science* 344(6191), 1489 (2014)

74. A. B. Fowler, F. F. Fang, W. E. Howard, and P. J. Stiles, Magneto-oscillatory conductance in silicon surfaces, *Phys. Rev. Lett.* 16(20), 901 (1966)

75. D. Jariwala, V. K. Sangwan, L. J. Lauhon, T. J. Marks, and M. C. Hersam, Emerging device applications for semiconducting two-dimensional transition metal dichalcogenides, *ACS Nano* 8(2), 1102 (2014)

76. Y. Liu, N. O. Weiss, X. Duan, H. C. Cheng, Y. Huang, and X. Duan, Van der Waals heterostructures and devices, *Nat. Rev. Mater.* 1(9), 16042 (2016)

77. W. Choi, N. Choudhary, G. H. Han, J. Park, D. Akinwande, and Y. H. Lee, Recent development of two-dimensional transition metal dichalcogenides and their applications, *Mater. Today* 20(3), 116 (2017)

78. M. M. Furchi, D. K. Polyushkin, A. Pospischil, and T. Mueller, Mechanisms of photoconductivity in atomically thin MoS_2, *Nano Lett.* 14(11), 6165 (2014)

79. C.-C. Wu, D. Jariwala, V. K. Sangwan, T. J. Marks, M. C. Hersam, and L. J. Lauhon, Elucidating the photoresponse of ultrathin MoS_2 field-effect transistors by scanning photocurrent microscopy, *J. Phys. Chem. Lett.* 4(15), 2508 (2013)

80. S. L. Howell, D. Jariwala, C. C. Wu, K. S. Chen, V. K. Sangwan, J. Kang, T. J. Marks, M. C. Hersam, and L. J. Lauhon, Investigation of band-offsets at monolayer–multilayer MoS_2 junctions by scanning photocurrent microscopy, *Nano Lett.* 15(4), 2278 (2015)

81. M. Tosun, D. Fu, S. B. Desai, C. Ko, J. Seuk Kang, D. H. Lien, M. Najmzadeh, S. Tongay, J. Wu, and A. Javey, MoS_2 heterojunctions by thickness modulation, *Sci. Rep.* 5(1), 10990 (2015)

82. H. Zeng, J. Dai, W. Yao, D. Xiao, and X. Cui, Valley polarization in MoS_2 monolayers by optical pumping, *Nat. Nanotechnol.* 7(8), 490 (2012)

83. T. Cao, G. Wang, W. Han, H. Ye, C. Zhu, J. Shi, Q. Niu, P. Tan, E. Wang, B. Liu, and J. Feng, Valley-selective circular dichroism of monolayer molybdenum disulphide, *Nat. Commun.* 3(1), 887 (2012)

84. T. Korn, S. Heydrich, M. Hirmer, J. Schmutzler, and C. Schüller, Low-temperature photocarrier dynamics in monolayer MoS_2, *Appl. Phys. Lett.* 99(10), 102109 (2011)

85. G. Wang, L. Bouet, D. Lagarde, M. Vidal, A. Balocchi, T. Amand, X. Marie, and B. Urbaszek, Valley dynamics probed through charged and neutral exciton emission in monolayer WSe_2, *Phys. Rev. B* 90(7), 075413 (2014)

86. D. Lagarde, L. Bouet, X. Marie, C. Zhu, B. Liu, T. Amand, P. Tan, and B. Urbaszek, Carrier and polarization dynamics in monolayer MoS_2, *Phys. Rev. Lett.* 112(4), 047401 (2014)

87. G. Wang, E. Palleau, T. Amand, S. Tongay, X. Marie, and B. Urbaszek, Polarization and time-resolved photoluminescence spectroscopy of excitons in $MoSe_2$ monolayers, *Appl. Phys. Lett.* 106(11), 112101 (2015)

88. C. Robert, D. Lagarde, F. Cadiz, G. Wang, B. Lassagne, T. Amand, A. Balocchi, P. Renucci, S. Tongay, B. Urbaszek, and X. Marie, Exciton radiative lifetime in transition metal dichalcogenide monolayers, *Phys. Rev. B* 93(20), 205423 (2016)

89. G. Plechinger, P. Nagler, A. Arora, R. Schmidt, A. Chernikov, J. Lupton, R. Bratschitsch, C. Schller, and T. Korn, Valley dynamics of excitons in monolayer dichalcogenides, *physica status solidi RRL* 11, 1700131 (2017)

90. L. Yang, N. A. Sinitsyn, W. Chen, J. Yuan, J. Zhang, J. Lou, and S. A. Crooker, Long-lived nanosecond spin relaxation and spin coherence of electrons in monolayer MoS_2 and WS_2, *Nat. Phys.* 11(10), 830 (2015)

91. X. Song, S. Xie, K. Kang, J. Park, and V. Sih, Long-lived hole spin/valley polarization probed by Kerr rotation in monolayer WSe_2, *Nano Lett.* 16(8), 5010 (2016)

92. T. Yan, S. Yang, D. Li, and X. Cui, Long valley relaxation time of free carriers in monolayer WSe_2, *Phys. Rev. B* 95(24), 241406 (2017)

93. P. Dey, L. Yang, C. Robert, G. Wang, B. Urbaszek, X. Marie, and S. A. Crooker, Gate-controlled spin-valley locking of resident carriers in WSe_2 monolayers, *Phys. Rev. Lett.* 119(13), 137401 (2017)

94. G. Aivazian, Z. Gong, A. M. Jones, R.L. Chu, J. Yan, D. G. Mandrus, C. Zhang, D. Cobden, W. Yao, and X. Xu, Magnetic control of valley pseudospin in monolayer WSe_2, *Nat. Phys.* 11, 148 (2015)

95. A. Srivastava, M. Sidler, A. V. Allain, D. S. Lembke, A. Kis, and A. Imamoğlu, Valley Zeeman effect in elementary optical excitations of monolayer WSe_2, *Nat. Phys.* 11(2), 141 (2015)

96. Y. Li, J. Ludwig, T. Low, A. Chernikov, X. Cui, G. Arefe, Y. D. Kim, A. M. van der Zande, A. Rigosi, H. M. Hill, S. H. Kim, J. Hone, Z. Li, D. Smirnov, and T. F. Heinz, Valley splitting and polarization by the Zeeman effect in monolayer $MoSe_2$, *Phys. Rev. Lett.* 113(26), 266804 (2014)

97. D. MacNeill, C. Heikes, K. F. Mak, Z. Anderson, A. Kormányos, V. Zólyomi, J. Park, and D. C. Ralph, Breaking of valley degeneracy by magnetic field in monolayer $MoSe_2$, *Phys. Rev. Lett.* 114(3), 037401 (2015)

98. M. Molas, C. Faugeras, A. Slobodeniuk, K. Nogajewski, M. Bartos, D. Basko, and M. Potemski, Brightening of dark excitons in monolayers of semiconducting transition metal dichalcogenides, *2D Materials* 4, 021003 (2017)

99. G. Wang, M. M. Glazov, C. Robert, T. Amand, X. Marie, and B. Urbaszek, Double resonant Raman scattering and valley coherence generation in monolayer WSe_2, *Phys. Rev. Lett.* 115(11), 117401 (2015)

100. G. Wang, X. Marie, B. L. Liu, T. Amand, C. Robert, F. Cadiz, P. Renucci, and B. Urbaszek, Control of exciton valley coherence in transition metal dichalcogenide monolayers, *Phys. Rev. Lett.* 117(18), 187401 (2016)

101. Z. Ye, D. Sun, and T. F. Heinz, Optical manipulation of valley pseudospin, *Nat. Phys.* 13, 26 (2016)

102. R. Schmidt, A. Arora, G. Plechinger, P. Nagler, A. G. del Águila, M. V. Ballottin, P. C. Christianen, S. M. de Vasconcellos, C. Schüller, T. Korn, and R. Bratschitsch, Magnetic-field-induced rotation of polarized light emission from monolayer WS_2, *Phys. Rev. Lett.* 117(7), 077402 (2016)

103. F. Cadiz, E. Courtade, C. Robert, G. Wang, Y. Shen, H. Cai, T. Taniguchi, K. Watanabe, H. Carrere, D. Lagarde, M. Manca, T. Amand, P. Renucci, S. Tongay, X. Marie, and B. Urbaszek, Excitonic linewidth approaching the homogeneous limit in MoS_2-based van der Waals heterostructures, *Phys. Rev. X* 7(2), 021026 (2017)

104. N. Yoshikawa, S. Tani, and K. Tanaka, Raman-like resonant secondary emission causes valley coherence in CVD-grown monolayer MoS_2, *Phys. Rev. B* 95(11), 115419 (2017)

105. K. Hao, G. Moody, F.Wu, C. K. Dass, L. Xu, C.-H. Chen, L. Sun, M.-Y. Li, L.-J. Li, A. H. MacDonald, and X. Li, Direct measurement of exciton valley coherence in monolayer WSe_2, *Nat. Phys.* 12, 677 (2016)

106. N. Ubrig, S. Jo, M. Philippi, D. Costanzo, H. Berger, A. B. Kuzmenko, and A. F. Morpurgo, Microscopic origin of the valley Hall effect in transition metal dichalcogenides revealed by wavelength-dependent mapping, *Nano Lett.* 17(9), 5719 (2017)

107. M. Onga, Y. Zhang, T. Ideue, and Y. Iwasa, Exciton Hall effect in monolayer MoS_2, *Nat. Mater.* 16(12), 1193 (2017)

108. J. Lee, Z. Wang, H. Xie, K. F. Mak, and J. Shan, Valley magnetoelectricity in single-layer MoS_2, *Nat. Mater.* 16(9), 887 (2017)

109. Y. Kato, R. Myers, A. Gossard, and D. Awschalom, Observation of the spin Hall effect in semiconductors, *Science* 306(5703), 1910 (2004)

110. M. Glazov and S. Ganichev, High frequency electric field induced nonlinear effects in graphene, *Phys. Rep.* 535(3), 101 (2014)

111. M. Eginligil, B. Cao, Z. Wang, X. Shen, C. Cong, J. Shang, C. Soci, and T. Yu, Dichroic spin–valley photocurrent in monolayer molybdenum disulphide, *Nat. Commun.* 6, 7636 (2015)

112. H. Guan, N. Tang, X. Xu, L. Shang, W. Huang, L. Fu, X. Fang, J. Yu, C. Zhang, X. Zhang, L. Dai, Y. Chen, W. Ge, and B. Shen, Photon wavelength dependent valley photocurrent in multilayer MoS_2, *Phys. Rev. B* 96(24), 241304 (2017)

113. H. Yuan, X. Wang, B. Lian, H. Zhang, X. Fang, B. Shen, G. Xu, Y. Xu, S. C. Zhang, H. Y. Hwang, and Y. Cui, Generation and electric control of spin–valley-coupled circular photogalvanic current in WSe_2, *Nat. Nanotechnol.* 9(10), 851 (2014)

114. A. V. Stier, N. P. Wilson, G. Clark, X. Xu, and S. A. Crooker, Probing the influence of dielectric environment on excitons in monolayer WSe_2: Insight from high magnetic fields, *Nano Lett.* 16(11), 7054 (2016)

115. M. Buscema, G. A. Steele, H. S. van der Zant, and A. Castellanos-Gomez, The effect of the substrate on the Raman and photoluminescence emission of single-layer MoS_2, *Nano Res.* 7(4), 561 (2014)

116. S. Latini, T. Olsen, and K. S. Thygesen, Excitons in van der Waals heterostructures: The important role of dielectric screening, *Phys. Rev. B* 92(24), 245123 (2015)

117. H. Isago, Optical Spectra of Phthalocyanines and Related Compounds, Springer, 2015

118. X. Ling, W. Fang, Y. H. Lee, P. T. Araujo, X. Zhang, J. F. Rodriguez-Nieva, Y. Lin, J. Zhang, J. Kong, and M. S. Dresselhaus, Raman enhancement effect on two-dimensional layered materials: Graphene, h-BN and MoS_2, *Nano Lett.* 14(6), 3033 (2014)

119. C. Muehlethaler, C. R. Considine, V. Menon, W. C. Lin, Y.H. Lee, and J. R. Lombardi, Ultrahigh Raman enhancement on monolayer MoS_2, *ACS Photon.* 3(7), 1164 (2016)

120. J. F. Arenas, M. S. Woolley, J. C. Otero, and J. I. Marcos, Charge-transfer processes in surface-enhanced Raman scattering, Franck–Condon active vibrations of pyrazine, *J. Phys. Chem.* 100(8), 3199 (1996)

121. D. Jariwala, S. L. Howell, K. S. Chen, J. Kang, V. K. Sangwan, S. A. Filippone, R. Turrisi, T. J. Marks, L. J. Lauhon, and M. C. Hersam, Hybrid, gate-tunable, van der Waals p–n heterojunctions from pentacene and MoS_2, *Nano Lett.* 16(1), 497 (2016)

122. A. Raja, A. Montoya-Castillo, J. Zultak, X. X. Zhang, Z. Ye, C. Roquelet, D. A. Chenet, A. M. van der Zande, P. Huang, S. Jockusch, J. Hone, D. R. Reichman, L. E. Brus, and T. F. Heinz, Energy transfer from quantum dots to graphene and MoS_2: The role of absorption and screening in two-dimensional materials, *Nano Lett.* 16(4), 2328 (2016)

123. T. Guo, S. Sampat, K. Zhang, J. A. Robinson, S. M. Rupich, Y. J. Chabal, Y. N. Gartstein, and A. V. Malko, Order of magnitude enhancement of monolayer MoS_2 photoluminescence due to near-field energy influx from nanocrystal films, *Sci. Rep.* 7, 41967 (2017)

124. S. H. Yu, Y. Lee, S. K. Jang, J. Kang, J. Jeon, C. Lee, J. Y. Lee, H. Kim, E. Hwang, S. Lee, and J. H. Cho, Dye-sensitized MoS_2 photodetector with enhanced spectral photoresponse, *ACS Nano* 8(8), 8285 (2014)

125. S. Bettis Homan, V. K. Sangwan, I. Balla, H. Bergeron, E. A. Weiss, and M. C. Hersam, Ultrafast exciton dissociation and long-lived charge separation in a photovoltaic Pentacene–MoS_2 van der Waals heterojunction, *Nano Lett.* 17(1), 164 (2017)

126. F. Prins, A. J. Goodman, and W. A. Tisdale, Reduced dielectric screening and enhanced energy transfer in single- and few-layer MoS_2, *Nano Lett.* 14(11), 6087 (2014)

127. D. Prasai, A. R. Klots, A. Newaz, J. S. Niezgoda, N. J. Orfield, C. A. Escobar, A. Wynn, A. Efimov, G. K. Jennings, S. J. Rosenthal, and K. I. Bolotin, Electrical control of near-field energy transfer between quantum dots and two-dimensional semiconductors, *Nano Lett.* 15(7), 4374 (2015)

128. M. Amani, D. H. Lien, D. Kiriya, J. Xiao, A. Azcatl, J. Noh, S. R. Madhvapathy, R. Addou, K. C. Santosh, M. Dubey, et al., Near-unity photoluminescence quantum yield in MoS_2, *Science* 350(6264), 1065 (2015)

129. D. M. Sim, M. Kim, S. Yim, M.J. Choi, J. Choi, S. Yoo, and Y. S. Jung, Controlled doping of vacancy-containing few-layer MoS_2 *via* highly stable thiol-based molecular chemisorption, *ACS Nano* 9(12), 12115 (2015)

130. H. V. Han, A. Y. Lu, L. S. Lu, J. K. Huang, H. Li, C. L. Hsu, Y. C. Lin, M. H. Chiu, K. Suenaga, C. W. Chu, H. C. Kuo, W. H. Chang, L. J. Li, and Y. Shi, Photoluminescence enhancement and structure repairing of monolayer $MoSe_2$ by hydrohalic acid treatment, *ACS Nano* 10(1), 1454 (2016)

131. I. S. Kim, V. K. Sangwan, D. Jariwala, J. D. Wood, S. Park, K.S. Chen, F. Shi, F. Ruiz-Zepeda, A. Ponce, M. Jose-Yacaman, V. P. Dravid, T. J. Marks, M. C. Hersam, and L. J. Lauhon, Influence of stoichiometry on the optical and electrical properties of chemical vapor deposition derived MoS_2, *ACS Nano* 8(10), 10551 (2014)

132. X. Liu, D. Qu, J. Ryu, F. Ahmed, Z. Yang, D. Lee, and W. J. Yoo, P-type polar transition of chemically doped multilayer MoS_2 transistor, *Adv. Mater.* 28(12), 2345 (2016)

133. A. Nipane, D. Karmakar, N. Kaushik, S. Karande, and S. Lodha, Few-layer MoS_2 *p*-type devices enabled by selective doping using low energy phosphorus implantation, *ACS Nano* 10(2), 2128 (2016)

134. C.-H. Chen, C.-L. Wu, J. Pu, M.-H. Chiu, P. Kumar, T. Takenobu, and L.-J. Li, Hole mobility enhancement and *p*-doping in monolayer WSe_2 by gold decoration, *2D Materials* 1, 034001 (2014)

135. H. Matsuoka, K. Kanahashi, N. Tanaka, Y. Shoji, L. J. Li, J. Pu, H. Ito, H. Ohta, T. Fukushima, and T. Takenobu, Chemical hole doping into large-area transition metal dichalcogenide monolayers using boron-based oxidant, *Jpn. J. Appl. Phys.* 57(2S2), 02CB15 (2018)

136. T. Komesu, D. Le, I. Tanabe, E. F. Schwier, Y. Kojima, M. Zheng, K. Taguchi, K. Miyamoto, T. Okuda, H. Iwasawa, K. Shimada, T. S. Rahman, and P. A. Dowben, Adsorbate doping of MoS_2 and WSe_2: The influence of Na and Co, *J. Phys.: Condens. Matter* 29(28), 285501 (2017)

137. H. Fang, M. Tosun, G. Seol, T. C. Chang, K. Takei, J. Guo, and A. Javey, Degenerate n-doping of few-layer transition metal dichalcogenides by potassium, *Nano Lett.* 13(5), 1991 (2013)

138. K. Chen, D. Kiriya, M. Hettick, M. Tosun, T.J. Ha, S. R. Madhvapathy, S. Desai, A. Sachid, and A. Javey, Air stable n-doping of WSe_2 by silicon nitride thin films with tunable fixed charge density, *APL Mater.* 2, 092504 (2014)

139. W. Wang, X. Niu, H. Qian, L. Guan, M. Zhao, X. Ding, S. Zhang, Y. Wang, and J. Sha, Surface charge transfer doping of monolayer molybdenum disulfide by black phosphorus quantum dots, *Nanotechnology* 27(50), 505204 (2016)

140. S. S. Chee, C. Oh, M. Son, G. C. Son, H. Jang, T. J. Yoo, S. Lee, W. Lee, J. Y. Hwang, H. Choi, B. H. Lee, and M. H. Ham, Sulfur vacancy-induced reversible doping

of transition metal disulfides via hydrazine treatment, *Nanoscale* 9(27), 9333 (2017)

141. P. Nagler, M. V. Ballottin, A. A. Mitioglu, F. Mooshammer, N. Paradiso, C. Strunk, R. Huber, A. Chernikov, P. Christianen, C. Schüller, and T. Korn, Giant magnetic splitting inducing near-unity valley polarization in van der Waals heterostructures, *Nat. Commun.* 8(1), 1551 (2017)

142. P. Rivera, K. L. Seyler, H. Yu, J. R. Schaibley, J. Yan, D. G. Mandrus, W. Yao, and X. Xu, Valley-polarized exciton dynamics in a 2D semiconductor heterostructure, *Science* 351(6274), 688 (2016)

143. J. Kang, S. Tongay, J. Zhou, J. Li, and J. Wu, Band offsets and heterostructures of two-dimensional semiconductors, *Appl. Phys. Lett.* 102(1), 012111 (2013)

144. M. Y. Li, Y. Shi, C. C. Cheng, L. S. Lu, Y. C. Lin, H. L. Tang, M. L. Tsai, C. W. Chu, K. H. Wei, J. H. He, W.H. Chang, K. Suenaga, and L.J. Li, Epitaxial growth of a monolayer WSe_2-MoS_2 lateral p-n junction with an atomically sharp interface, *Science* 349(6247), 524 (2015)

145. R. Cheng, D. Li, H. Zhou, C. Wang, A. Yin, S. Jiang, Y. Liu, Y. Chen, Y. Huang, and X. Duan, Electroluminescence and photocurrent generation from atomically sharp WSe_2/MoS_2 heterojunction *p–n* diodes, *Nano Lett.* 14(10), 5590 (2014)

146. M. M. Furchi, A. A. Zechmeister, F. Hoeller, S. Wachter, A. Pospischil, and T. Mueller, Photovoltaics in van der Waals heterostructures, *IEEE J. Sel. Top. Quantum Electron.* 23(1), 106 (2017)

147. B. Peng, G. Yu, X. Liu, B. Liu, X. Liang, L. Bi, L. Deng, T. C. Sum, and K. P. Loh, Ultrafast charge transfer in MoS_2/WSe_2 p–n Heterojunction, *2D Materials* 3, 025020 (2016)

148. J. Kim, C. Jin, B. Chen, H. Cai, T. Zhao, P. Lee, S. Kahn, K. Watanabe, T. Taniguchi, S. Tongay, M. F. Crommie, and F. Wang, Observation of ultralong valley lifetime in WSe_2/MoS_2 heterostructures, *Sci. Adv.* 3(7), e1700518 (2017)

149. J. R. Schaibley, P. Rivera, H. Yu, K. L. Seyler, J. Yan, D. G. Mandrus, T. Taniguchi, K. Watanabe, W. Yao, and X. Xu, Directional interlayer spin-valley transfer in two-dimensional heterostructures, *Nat. Commun.* 7, 13747 (2016)

150. H. Fang, C. Battaglia, C. Carraro, S. Nemsak, B. Ozdol, J. S. Kang, H. A. Bechtel, S. B. Desai, F. Kronast, A. A. Unal, et al., Strong interlayer coupling in van der Waals heterostructures built from single-layer chalcogenides, *Proc. Natl. Acad. Sci. USA* 111(17), 6198 (2014)

151. P. Rivera, J. Schaibley, A. Jones, J. Ross, S. Wu, G. Aivazian, P. Klement, K. Seyler, G. Clark, N. Ghimire, J. Yan, D. G. Mandrus, W. Yao, and X. Xu, Observation of long-lived interlayer excitons in monolayer $MoSe_2$–WSe_2 heterostructures, *Nat. Commun.* 6(1), 6242 (2015)

152. P. K. Nayak, Y. Horbatenko, S. Ahn, G. Kim, J.U. Lee, K. Y. Ma, A.R. Jang, H. Lim, D. Kim, S. Ryu, H. Cheong, N. Park, and H. S. Shin, Probing evolution of twist-angle-dependent interlayer excitons in $MoSe_2/WSe_2$ van der Waals heterostructures, *ACS Nano* 11, 4041 (2017)

153. J. S. Ross, P. Rivera, J. Schaibley, E. Lee-Wong, H. Yu, T. Taniguchi, K. Watanabe, J. Yan, D. Mandrus, D. Cobden, W. Yao, and X. Xu, Interlayer exciton optoelectronics in a 2D heterostructure p–n junction, *Nano Lett.* 17(2), 638 (2017)

154. S. Huang, L. Liang, X. Ling, A. A. Puretzky, D. B. Geohegan, B. G. Sumpter, J. Kong, V. Meunier, and M. S. Dresselhaus, Low-frequency interlayer Raman modes to probe interface of twisted bilayer MoS_2, *Nano Lett.* 16(2), 1435 (2016)

155. K. Liu, L. Zhang, T. Cao, C. Jin, D. Qiu, Q. Zhou, A. Zettl, P. Yang, S. G. Louie, and F. Wang, Evolution of interlayer coupling in twisted molybdenum disulfide bilayers, *Nat. Commun.* 5, 4966 (2014)

156. S. Huang, X. Ling, L. Liang, J. Kong, H. Terrones, V. Meunier, and M. S. Dresselhaus, Probing the interlayer coupling of twisted bilayer MoS_2 using photoluminescence spectroscopy, *Nano Lett.* 14(10), 5500 (2014)

157. J. Xia, X. Wang, B. K. Tay, S. Chen, Z. Liu, J. Yan, and Z. Shen, Valley polarization in stacked MoS_2 induced by circularly polarized light, *Nano Res.* 10(5), 1618 (2017)

158. R. Suzuki, M. Sakano, Y. J. Zhang, R. Akashi, D. Morikawa, A. Harasawa, K. Yaji, K. Kuroda, K. Miyamoto, T. Okuda, K. Ishizaka, R. Arita, and Y. Iwasa, Valley-dependent spin polarization in bulk MoS_2 with broken inversion symmetry, *Nat. Nanotechnol.* 9(8), 611 (2014)

159. T. Jiang, H. Liu, D. Huang, S. Zhang, Y. Li, X. Gong, Y. R. Shen, W. T. Liu, and S. Wu, Valley and band structure engineering of folded MoS_2 bilayers, *Nat. Nanotechnol.* 9(10), 825 (2014)

160. B. Miller, A. Steinhoff, B. Pano, J. Klein, F. Jahnke, A. Holleitner, and U. Wurstbauer, Long-lived direct and indirect interlayer excitons in van der Waals heterostructures, *Nano Lett.* 17(9), 5229 (2017)

161. H. Yu, Y. Wang, Q. Tong, X. Xu, and W. Yao, Anomalous light cones and valley optical selection rules of interlayer excitons in twisted heterobilayers, *Phys. Rev. Lett.* 115(18), 187002 (2015)

162. M. Gmitra, S. Konschuh, C. Ertler, C. Ambrosch-Draxl, and J. Fabian, Band-structure topologies of graphene: Spin-orbit coupling effects from first principles, *Phys. Rev. B* 80(23), 235431 (2009)

163. Y. K. Luo, J. Xu, T. Zhu, G. Wu, E. J. McCormick, W. Zhan, M. R. Neupane, and R. K. Kawakami, Opto-valleytronic spin injection in monolayer MoS_2/few-layer graphene hybrid spin valves, *Nano Lett.* 17(6), 3877 (2017)

164. A. Avsar, D. Unuchek, J. Liu, O. L. Sanchez, K. Watanabe, T. Taniguchi, B. Ozyilmaz, and A. Kis, Optospintronics in graphene via proximity coupling, *ACS Nano* 11(11), 11678 (2017)

165. A. Avsar, J. Y. Tan, T. Taychatanapat, J. Balakrishnan, G. Koon, Y. Yeo, J. Lahiri, A. Carvalho, A. Rodin, E. C. T. O'Farrell, G. Eda, A. H. Castro Neto, and B. Özyilmaz, Spin–orbit proximity effect in graphene, *Nat. Commun.* 5, 4875 (2014)

166. M. Gmitra, D. Kochan, P. Högl, and J. Fabian, Trivial and inverted Dirac bands and the emergence of quantum spin Hall states in graphene on transition-metal dichalcogenides, *Phys. Rev. B* 93(15), 155104 (2016)

167. S. Omar and B. J. van Wees, Graphene-WS_2 heterostructures for tunable spin injection and spin transport, *Phys. Rev. B* 95(8), 081404 (2017)

168. T. S. Ghiasi, J. Ingla-Aynés, A. A. Kaverzin, and B. J. van Wees, Large proximity-induced spin lifetime anisotropy in transition-metal dichalcogenide/graphene heterostructures, *Nano Lett.* 17(12), 7528 (2017) (2017)

169. A. W. Cummings, J. H. Garcia, J. Fabian, and S. Roche, Giant spin lifetime anisotropy in graphene induced by proximity effects, *Phys. Rev. Lett.* 119(20), 206601 (2017)

170. L. A. Benítez, J. F. Sierra, W. S. Torres, A. Arrighi, F. Bonell, M. V. Costache, and S. O. Valenzuela, Strongly anisotropic spin relaxation in graphene–transition metal dichalcogenide heterostructures at room temperature, *Nat. Phys.* 14, 303 (2017)

171. S. Omar and B. J. van Wees, Spin transport in high-mobility graphene on WS_2 substrate with electric-field tunable proximity spin-orbit interaction, *Phys. Rev. B* 97(4), 045414 (2018)

172. W. Yan, O. Txoperena, R. Llopis, H. Dery, L. E. Hueso, and F. Casanova, A two-dimensional spin field-effect switch, *Nat. Commun.* 7, 13372 (2016)

173. A. Dankert and S. P. Dash, Electrical gate control of spin current in van der Waals heterostructures at room temperature, *Nat. Commun.* 8, 16093 (2017)

174. D. Sercombe, S. Schwarz, O. Del Pozo-Zamudio, F. Liu, B. Robinson, E. Chekhovich, I. Tartakovskii, O. Kolosov, and A. Tartakovskii, Optical investigation of the natural electron doping in thin MoS_2 films deposited on dielectric substrates, *Sci. Rep.* 3, 3489 (2013)

175. D. Lin, P. Fan, E. Hasman, and M. L. Brongersma, Dielectric gradient metasurface optical elements, *Science* 345(6194), 298 (2014)

176. M. K. L. Man, S. Deckoff-Jones, A. Winchester, G. Shi, G. Gupta, A. D. Mohite, S. Kar, E. Kioupakis, S. Talapatra, and K. M. Dani, Protecting the properties of monolayer MoS_2 on silicon based substrates with an atomically thin buffer, *Sci. Rep.* 6, 20890 (2016)

177. C. M. Chow, H. Yu, A. M. Jones, J. Yan, D. G. Mandrus, T. Taniguchi, K. Watanabe, W. Yao, and X. Xu, Unusual exciton–phonon interactions at van der Waals engineered interfaces, *Nano Lett.* 17(2), 1194 (2017)

178. W. J. Yu, Z. Li, H. Zhou, Y. Chen, Y. Wang, Y. Huang, and X. Duan, Vertically stacked multi-heterostructures of layered materials for logic transistors and complementary inverters, *Nat. Mater.* 12(3), 246 (2013)

179. J. Wierzbowski, J. Klein, F. Sigger, C. Straubinger, M. Kremser, T. Taniguchi, K. Watanabe, U. Wurstbauer, A. W. Holleitner, M. Kaniber, K. Mller, and J. J. Finley, Direct exciton emission from atomically thin transition metal dichalcogenide heterostructures near the lifetime limit, *Sci. Rep.* 7(1), 12383 (2017)

180. S. Tongay, J. Suh, C. Ataca, W. Fan, A. Luce, J. S. Kang, J. Liu, C. Ko, R. Raghunathanan, J. Zhou, et al., Optical signature of symmetry variations and spin-valley coupling in atomically thin tungsten dichalcogenides, *Sci. Rep.* 3, 1608 (2013)

181. J. Kunstmann, T. B. Wendumu, and G. Seifert, Localized defect states in MoS_2 monolayers: Electronic and optical properties, *physica status solidi (b)* 254, 1600645 (2016)

182. S. Y. Chen, T. Goldstein, J. Tong, T. Taniguchi, K. Watanabe, and J. Yan, Superior valley polarization and coherence of 2s excitons in monolayer WSe_2, *Phys. Rev. Lett.* 120(4), 046402 (2018)

183. K. Wang, K. D. Greve, L. A. Jauregui, A. Sushko, A. High, Y. Zhou, G. Scuri, T. Taniguchi, K. Watanabe, M. D. Lukin, H. Park, and P. Kim, Electrical control of charged carriers and excitons in atomically thin materials, *Nat. Nanotechnol.* 13(2), 128 (2018)

184. H. J. Conley, B. Wang, J. I. Ziegler, S. T. Jr Haglund, Pantelides, and K. I. Bolotin, Bandgap engineering of strained monolayer and bilayer MoS_2, *Nano Lett.* 13(8), 3626 (2013)

185. S. B. Desai, G. Seol, J. S. Kang, H. Fang, C. Battaglia, R. Kapadia, J. W. Ager, J. Guo, and A. Javey, Strain-induced indirect to direct bandgap transition in multilayer WSe_2, *Nano Lett.* 14(8), 4592 (2014)

186. H. Rostami, R. Roldán, E. Cappelluti, R. Asgari, and F. Guinea, Theory of strain in single-layer transition metal dichalcogenides, *Phys. Rev. B* 92(19), 195402 (2015)

187. A. Branny, S. Kumar, R. Proux, and B. D. Gerardot, Deterministic strain-induced arrays of quantum emitters in a two-dimensional semiconductor, *Nat. Commun.* 8, 15053 (2017)

188. M. Koperski, K. Nogajewski, A. Arora, V. Cherkez, P. Mallet, J. Y. Veuillen, J. Marcus, P. Kossacki, and M. Potemski, Single photon emitters in exfoliated WSe_2 structures, *Nat. Nanotechnol.* 10(6), 503 (2015)

189. C. Palacios-Berraquero, D. M. Kara, A. R. P. Montblanch, M. Barbone, P. Latawiec, D. Yoon, A. K. Ott, M. Loncar, A. C. Ferrari, and M. Atatüre, Large-scale quantum-emitter arrays in atomically thin semiconductors, *Nat. Commun.* 8, 15093 (2017)

190. G. D. Shepard, O. A. Ajayi, X. Li, X.-Y. Zhu, J. Hone, and S. Strauf, Nanobubble induced formation of quantum emitters in monolayer semiconductors, *2D Materials* 4, 021019 (2017)

191. S. Schwarz, A. Kozikov, F. Withers, J. Maguire, A. Foster, S. Dufferwiel, L. Hague, M. Makhonin, L. Wilson, A. Geim, et al., Electrically pumped single-defect light emitters in WSe_2, *2D Materials* 3, 025038 (2016)

192. G. Clark, J. R. Schaibley, J. Ross, T. Taniguchi, K. Watanabe, J. R. Hendrickson, S. Mou, W. Yao, and X. Xu, Single defect light-emitting diode in a van der Waals heterostructure, *Nano Lett.* 16(6), 3944 (2016)

193. E. M. Mannebach, C. Nyby, F. Ernst, Y. Zhou, J. Tolsma, Y. Li, M. J. Sher, I. C. Tung, H. Zhou, Q. Zhang, et al., Dynamic optical tuning of interlayer interactions in the transition metal dichalcogenides, *Nano Lett.* 17(12), 7761 (2017)

194. S. A. Empedocles, D. J. Norris, and M. G. Bawendi, Photoluminescence spectroscopy of single CdSe nanocrystallite quantum dots, *Phys. Rev. Lett.* 77(18), 3873 (1996)

195. A. Imamoḡlu, H. Schmidt, G. Woods, and M. Deutsch, Strongly interacting photons in a nonlinear cavity, *Phys. Rev. Lett.* 79(8), 1467 (1997)

196. J. K. Furdyna and J. Kossut (Eds.), Diluted Magnetic Semiconductors, Semiconductors and Semimetals, Vol. 25 New York: Academic Press, 1988

197. D. R. Yakovlev and W. Ossau, in: Introduction to the Physics of Diluted Magnetic Semiconductors, Springer Series in Materials Science, Vol. 144, edited by J. A. Gaj and J. Kossut, Berlin Heidelberg: Springer, 2010, pp 221–262

198. R. C. Myers, M. Poggio, N. P. Stern, A. C. Gossard, and D. D. Awschalom, Antiferromagnetic s-d exchange coupling in GaMnAs, *Phys. Rev. Lett.* 95(1), 017204 (2005)

199. N. P. Stern, R. C. Myers, M. Poggio, A. C. Gossard, and D. D. Awschalom, Confinement engineering of s-d exchange interactions in $Ga_{1-x}Mn_xAs/Al_yGa_{1-y}As$ quantum wells, *Phys. Rev. B* 75(4), 045329 (2007)

200. R. Beaulac, L. Schneider, P. I. Archer, G. Bacher, and D. R. Gamelin, Light-induced spontaneous magnetization in doped colloidal quantum dots, *Science* 325(5943), 973 (2009)

201. T. Ando, A. B. Fowler, and F. Stern, Electronic properties of two-dimensional systems, *Rev. Mod. Phys.* 54(2), 437 (1982)

202. U. K. Mishra, P. Parikh, and Y. F. Wu, AlGaN/GaN HEMTs-an overview of device operation and applications, *Proc. IEEE* 90(6), 1022 (2002)

203. D. C. Tsui, H. L. Stormer, and A. C. Gossard, Two-dimensional magnetotransport in the extreme quantum limit, *Phys. Rev. Lett.* 48(22), 1559 (1982)

204. Q. Sun, Y. A. Wang, L. S. Li, D. Wang, T. Zhu, J. Xu, C. Yang, and Y. Li, Bright, multicoloured light-emitting diodes based on quantum dots, *Nat. Photon.* 1(12), 717 (2007)

205. I. J. Kramer and E. H. Sargent, The architecture of colloidal quantum dot solar cells: Materials to devices, *Chem. Rev.* 114(1), 863 (2014)

206. H. M. Azzazy, M. M. Mansour, and S. C. Kazmierczak, From diagnostics to therapy: Prospects of quantum dots, *Clin. Biochem.* 40(13–14), 917 (2007)

207. J. Klinovaja and D. Loss, Spintronics in MoS_2 monolayer quantum wires, *Phys. Rev. B* 88(7), 075404 (2013)

208. V. Mourik, K. Zuo, S. M. Frolov, S. Plissard, E. Bakkers, and L. P. Kouwenhoven, Signatures of Majorana fermions in hybrid superconductor-semiconductor nanowire devices, *Science* 336(6084), 1003 (2012)

209. S. Pavlović and F. M. Peeters, Electronic properties of triangular and hexagonal MoS_2 quantum dots, *Phys. Rev. B* 91, 155410 (2015)

210. L. Pei, S. Tao, S. Haibo, and X. Song, Structural stability, electronic and magnetic properties of MoS_2 quantum dots based on the first principles, *Solid State Commun.* 218, 25 (2015)

211. A. J. Pearce and G. Burkard, Electron spin relaxation in a transition-metal dichalcogenide quantum dot, *2D Materials* 4, 025114 (2017)

212. M. Brooks and G. Burkard, Spin-degenerate regimes for single quantum dots in transition metal dichalcogenide monolayers, *Phys. Rev. B* 95(24), 245411 (2017)

213. S. Ono and T. Ogura, Theory of laterally confined two dimensional excitons, arXiv: 1801.06923 (2018)

214. G. Seifert, H. Terrones, M. Terrones, G. Jungnickel, and T. Frauenheim, Structure and electronic properties of MoS_2 nanotubes, *Phys. Rev. Lett.* 85(1), 146 (2000)

215. M. Remskar, A. Mrzel, Z. Skraba, A. Jesih, M. Ceh, J. Demšar, P. Stadelmann, F. Lévy, and D. Mihailovic, Self-assembly of subnanometer-diameter single-wall MoS_2 nanotubes, *Science* 292(5516), 479 (2001)

216. Z. Gan, L. Liu, H. Wu, Y. Hao, Y. Shan, X. Wu, and P. K. Chu, Quantum confinement effects across two-dimensional planes in MoS_2 quantum dots, *Appl. Phys. Lett.* 106(23), 233113 (2015)

217. D. Gopalakrishnan, D. Damien, B. Li, H. Gullappalli, V. K. Pillai, P. M. Ajayan, and M. M. Shaijumon, Electrochemical synthesis of luminescent MoS_2 quantum dots, *Chem. Commun.* 51(29), 6293 (2015)

218. H. Jin, M. Ahn, S. Jeong, J. H. Han, D. Yoo, D. H. Son, and J. Cheon, Colloidal single-layer quantum dots with lateral confinement effects on 2D exciton, *J. Am. Chem. Soc.* 138(40), 13253 (2016)

219. H. Jin, B. Baek, D. Kim, F. Wu, J. D. Batteas, J. Cheon, and D. H. Son, Effects of direct solvent-quantum dot interaction on the optical properties of colloidal monolayer WS_2 quantum dots, *Nano Lett.* 17(12), 7471 (2017)

220. H. Xu, Z. Ding, C. T. Nai, Y. Bao, F. Cheng, S. J. R. Tan, and K. P. Loh, Controllable synthesis of 2D and 1D MoS_2 nanostructures on Au surface, *Adv. Funct. Mater.* 27, 1603887 (2017)

221. G. Wei, D. A. Czaplewski, E. J. Lenferink, T. K. Stanev, I. W. Jung, and N. P. Stern, Size-tunable lateral confinement in monolayer semiconductors, *Sci. Rep.* 7(1), 3324 (2017)

222. G. Wei, E. J. Lenferink, D. A. Czaplewski, and N. P. Stern, Width-dependent photoluminescence and anisotropic Raman spectroscopy from monolayer MoS_2 nanoribbons, arXiv: 1709.04001 (2017)

223. G. B. Liu, H. Pang, Y. Yao, and W. Yao, Intervalley coupling by quantum dot confinement potentials in monolayer transition metal dichalcogenides, *New J. Phys.* 16(10), 105011 (2014)

224. G. Wei, T. K. Stanev, D. A. Czewski, I. W. Jung, and N. P. Stern, Silicon-nitride photonic circuits interfaced with monolayer MoS_2, *Appl. Phys. Lett.* 107(9), 091112 (2015)

225. J. Kim, X. Hong, C. Jin, S. F. Shi, C. Y. S. Chang, M. H. Chiu, L. J. Li, and F. Wang, Ultrafast generation of pseudo-magnetic field for valley excitons in WSe_2 monolayers, *Science* 346(6214), 1205 (2014)

226. W. Liu, B. Lee, C. H. Naylor, H. S. Ee, J. Park, A. C. Johnson, and R. Agarwal, Strong exciton–plasmon coupling in MoS_2 coupled with plasmonic lattice, *Nano Lett.* 16(2), 1262 (2016)

227. N. Peimyoo, J. Shang, C. Cong, X. Shen, X. Wu, E. K. Yeow, and T. Yu, Nonblinking, intense two-dimensional light emitter: Monolayer WS_2 triangles, *ACS Nano* 7(12), 10985 (2013)

228. H. Wang, C. Zhang, and F. Rana, Ultrafast dynamics of defect-assisted electron–hole recombination in monolayer MoS_2, *Nano Lett.* 15(1), 339 (2015)

229. S. Pimputkar, J. S. Speck, S. P. DenBaars, and S. Nakamura, Prospects for LED lighting, *Nat. Photon.* 3(4), 180 (2009)

230. T. Fujii, Y. Gao, R. Sharma, E. Hu, S. DenBaars, and S. Nakamura, Increase in the extraction efficiency of GaN-based light-emitting diodes via surface roughening, *Appl. Phys. Lett.* 84(6), 855 (2004)

231. X. Gan, Y. Gao, K. F. Mak, X. Yao, R. J. Shiue, A. van der Zande, M. E. Trusheim, F. Hatami, T. F. Heinz, J. Hone, et al., Controlling the spontaneous emission rate of monolayer MoS_2 in a photonic crystal nanocavity, *Appl. Phys. Lett.* 103(18), 181119 (2013)

232. S. Wu, S. Buckley, A. M. Jones, J. S. Ross, N. J. Ghimire, J. Yan, D. G. Mandrus, W. Yao, F. Hatami, J. Vučković, A. Majumdar, and X. D. Xu, Control of two-dimensional excitonic light emission via photonic crystal, *2D Materials* 1, 011001 (2014)

233. S. Schwarz, S. Dufferwiel, P. Walker, F. Withers, A. Trichet, M. Sich, F. Li, E. Chekhovich, D. Borisenko, N. N. Kolesnikov, K. S. Novoselov, et al., Two-dimensional metal–chalcogenide films in tunable optical microcavities, *Nano Lett.* 14(12), 7003 (2014)

234. Y. J. Noori, Y. Cao, J. Roberts, C. Woodhead, R. Bernardo-Gavito, P. Tovee, and R. J. Young, Photonic crystals for enhanced light extraction from 2D materials, *ACS Photon.* 3(12), 2515 (2016)

235. J. C. Reed, A. Y. Zhu, H. Zhu, F. Yi, and E. Cubukcu, Wavelength tunable microdisk cavity light source with a chemically enhanced MoS_2 emitter, *Nano Lett.* 15(3), 1967 (2015)

236. T. Ren, P. Song, J. Chen, and K. P. Loh, Whisper gallery modes in monolayer tungsten disulfide-hexagonal boron nitride optical cavity, *ACS Photon.* 5(2), 353 (2018)

237. S. Hammer, H. M. Mangold, A. E. Nguyen, D. Martinez-Ta, S. Naghibi Alvillar, L. Bartels, and H. J. Krenner, Scalable and transfer-free fabrication of MoS_2/SiO_2 hybrid nanophotonic cavity arrays with quality factors exceeding 4000, *Sci. Rep.* 7(1), 7251 (2017)

238. S. Wu, S. Buckley, J. R. Schaibley, L. Feng, J. Yan, D. G. Mandrus, F. Hatami, W. Yao, J. Vučković, A. Majumdar, and X. Xu, Monolayer semiconductor nanocavity lasers with ultralow thresholds, *Nature* 520(7545), 69 (2015)

239. A. Alduino and M. Paniccia, Wiring electronics with light, *Nat. Photon.* 1(3), 153 (2007)

240. H. J. Caulfield and S. Dolev, Why future supercomputing requires optics, *Nat. Photon.* 4(5), 261 (2010)

241. E. Murphy, Enabling optical communication, *Nat. Photon.* 4(5), 287 (2010)

242. O. Salehzadeh, M. Djavid, N. H. Tran, I. Shih, and Z. Mi, Optically pumped two-dimensional MoS_2 lasers operating at room-temperature, *Nano Lett.* 15(8), 5302 (2015)

243. H. Fang, J. Liu, H. Li, L. Zhou, L. Liu, J. Li, X. Wang, T. F. Krauss, and Y. Wang, 1305 nm $MoTe_2$-on-silicon Laser, arXiv: 1710.01591 (2017)

244. Y. Li, J. Zhang, D. Huang, H. Sun, F. Fan, J. Feng, Z. Wang, and C. Ning, Room-temperature continuous-wave lasing from monolayer molybdenum ditelluride integrated with a silicon nanobeam cavity, *Nat. Nanotechnol.* 12(10), 987 (2017)

245. S. Strauf and F. Jahnke, Single quantum dot nanolaser, *Laser & Photon. Rev.* 5, 607 (2011)

246. C. Weisbuch, M. Nishioka, A. Ishikawa, and Y. Arakawa, Observation of the coupled exciton-photon mode splitting in a semiconductor quantum microcavity, *Phys. Rev. Lett.* 69(23), 3314 (1992)

247. R. Houdré, C. Weisbuch, R. P. Stanley, U. Oesterle, P. Pellandini, and M. Ilegems, Measurement of cavity-polariton dispersion curve from angle-resolved photoluminescence experiments, *Phys. Rev. Lett.* 73(15), 2043 (1994)

248. H. Deng, H. Haug, and Y. Yamamoto, Exciton-polariton Bose–Einstein condensation, *Rev. Mod. Phys.* 82(2), 1489 (2010)

249. H. Deng, G. Weihs, C. Santori, J. Bloch, and Y. Yamamoto, Condensation of semiconductor microcavity exciton polaritons, *Science* 298(5591), 199 (2002)

250. J. Kasprzak, M. Richard, S. Kundermann, A. Baas, P. Jeambrun, J. Keeling, F. Marchetti, M. H. Szymańska, R. André, J. L. Staehli, V. Savona, P. B. Littlewood, B. Deveaud, and L. S. Dang, Bose–Einstein condensation of exciton polaritons, *Nature* 443(7110), 409 (2006)

251. R. Balili, V. Hartwell, D. Snoke, L. Pfeiffer, and K. West, Bose-Einstein condensation of microcavity polaritons in a trap, *Science* 316(5827), 1007 (2007)

252. S. Christopoulos, G. B. H. Von Högersthal, A. Grundy, P. Lagoudakis, A. Kavokin, J. Baumberg, G. Christmann, R. Butté, E. Feltin, J. F. Carlin, and N. Grandjean, Room-temperature polariton lasing in semiconductor microcavities, *Phys. Rev. Lett.* 98(12), 126405 (2007)

253. J. Baumberg, A. Kavokin, S. Christopoulos, A. Grundy, R. Butté, G. Christmann, D. Solnyshkov, G. Malpuech, G. B. H. von Högersthal, E. Feltin, et al., Spontaneous polarization buildup in a room-temperature polariton laser, *Phys. Rev. Lett.* 101(13), 136409 (2008)

254. S. Kéna-Cohen and S. Forrest, Room-temperature polariton lasing in an organic single-crystal microcavity, *Nat. Photonics* 4(6), 371 (2010)

255. T. Guillet, M. Mexis, J. Levrat, G. Rossbach, C. Brimont, T. Bretagnon, B. Gil, R. Butté, N. Grandjean, L. Orosz, et al., Polariton lasing in a hybrid bulk ZnO microcavity, *Appl. Phys. Lett.* 99(16), 161104 (2011)

256. J. D. Plumhof, T. Stöferle, L. Mai, U. Scherf, and R. F. Mahrt, Room-temperature Bose–Einstein condensation of cavity exciton–polaritons in a polymer, *Nat. Mater.* 13(3), 247 (2014)

257. T. C. Lu, Y. Y. Lai, Y. P. Lan, S. W. Huang, J. R. Chen, Y. C. Wu, W. F. Hsieh, and H. Deng, Room temperature polariton lasing vs. photon lasing in a ZnO-based hybrid microcavity, *Opt. Express* 20(5), 5530 (2012)

258. P. Bhattacharya, T. Frost, S. Deshpande, M. Z. Baten, A. Hazari, and A. Das, Room temperature electrically injected polariton laser, *Phys. Rev. Lett.* 112(23), 236802 (2014)

259. T. Liew, A. Kavokin, and I. Shelykh, Optical circuits based on polariton neurons in semiconductor microcavities, *Phys. Rev. Lett.* 101(1), 016402 (2008)

260. A. Amo, T. C. H. Liew, C. Adrados, R. Houdré, E. Giacobino, A. V. Kavokin, and A. Bramati, Exciton–polariton spin switches, *Nat. Photon.* 4(6), 361 (2010)

261. D. Sanvitto and S. Kéna-Cohen, The road towards polaritonic devices, *Nat. Mater.* 15(10), 1061 (2016)

262. S. Dufferwiel, S. Schwarz, F. Withers, A. Trichet, F. Li, M. Sich, O. Del Pozo-Zamudio, C. Clark, A. Nalitov, D. Solnyshkov, et al., Exciton-polaritons in van der Waals heterostructures embedded in tunable microcavities, *Nat. Commun.* 6, 8579 (2015)

263. M. Sidler, P. Back, O. Cotlet, A. Srivastava, T. Fink, M. Kroner, E. Demler, and A. Imamoglu, Fermi polaron-polaritons in charge-tunable atomically thin semiconductors, *Nat. Phys.* 13(3), 255 (2016)

264. S. Dufferwiel, T. Lyons, D. Solnyshkov, A. Trichet, F. Withers, S. Schwarz, G. Malpuech, J. Smith, K. Novoselov, M. Skolnick, et al., Valley-addressable polaritons in atomically thin semiconductors, Nat. Photon. 11, 497 (2017)

265. L. C. Flatten, Z. He, D. M. Coles, A. A. P. Trichet, A. W. Powell, R. A. Taylor, J. H. Warner, and J. M. Smith, Room-temperature exciton-polaritons with two-dimensional WS_2, *Sci. Rep.* 6(1), 33134 (2016)

266. L. C. Flatten, D. M. Coles, Z. He, D. G. Lidzey, R. A. Taylor, J. H. Warner, and J. M. Smith, Electrically tunable organic–inorganic hybrid polaritons with monolayer WS_2, *Nat. Commun.* 8, 14097 (2017)

267. Z. Sun, J. Gu, A. Ghazaryan, Z. Shotan, C. R. Considine, M. Dollar, B. Chakraborty, X. Liu, P. Ghaemi, S. Kéna-Cohen, and V. M. Menon, Optical control of room-temperature valley polaritons, *Nat. Photon.* 11(8), 491 (2017)

268. X. Liu, W. Bao, Q. Li, C. Ropp, Y. Wang, and X. Zhang, Control of coherently coupled exciton polaritons in monolayer Tungsten disulphide, *Phys. Rev. Lett.* 119(2), 027403 (2017)

269. N. Lundt, S. Stoll, P. Nagler, A. Nalitov, S. Klembt, S. Betzold, J. Goddard, E. Frieling, A. Kavokin, C. Schüller, T. Korn, S. Höfling, and C. Schneider, Observation of macroscopic valley-polarized monolayer exciton-polaritons at room temperature, *Phys. Rev. B* 96(24), 241403 (2017)

270. L. Zhang, R. Gogna, W. Burg, E. Tutuc, and H. Deng, Photonic-crystal exciton-polaritons in monolayer semiconductors, *Nat. Commun.* 9, 713 (2018)

271. M. E. Sasin, R. P. Seisyan, M. A. Kalitteevski, S. Brand, R. A. Abram, J. M. Chamberlain, A. Y. Egorov, A. P. Vasil'ev, V. S. Mikhrin, and A. V. Kavokin, Tamm plasmon polaritons: Slow and spatially compact light, *Appl. Phys. Lett.* 92(25), 251112 (2008)

272. T. Hu, Y. Wang, L. Wu, L. Zhang, Y. Shan, J. Lu, J. Wang, S. Luo, Z. Zhang, L. Liao, S. Wu, X. Shen, and Z. Chen, Strong coupling between Tamm plasmon polariton and two dimensional semiconductor excitons, *Appl. Phys. Lett.* 110(5), 051101 (2017)

273. S. Wang, S. Li, T. Chervy, A. Shalabney, S. Azzini, E. Orgiu, J. A. Hutchison, C. Genet, P. Samorì, and T. W. Ebbesen, Coherent coupling of WS_2 monolayers with metallic photonic nanostructures at room temperature, *Nano Lett.* 16(7), 4368 (2016)

274. Z. Wang, R. Gogna, and H. Deng, What is the best planar cavity for maximizing coherent exciton-photon coupling, *Appl. Phys. Lett.* 111(6), 061102 (2017)

275. B. Zhang, Z. Wang, S. Brodbeck, C. Schneider, M. Kamp, S. Höing, and H. Deng, Zero-dimensional polariton laser in a subwavelength grating-based vertical microcavity, *Light Sci. Appl.* 3(1), e135 (2014)

276. S. Kim, B. Zhang, Z. Wang, J. Fischer, S. Brodbeck, M. Kamp, C. Schneider, S. Höing, and H. Deng, Coherent polariton laser, *Phys. Rev. X* 6(1), 011026 (2016)

277. G. Sallen, L. Bouet, X. Marie, G. Wang, C. Zhu, W. Han, Y. Lu, P. Tan, T. Amand, B. Liu, and B. Urbaszek, Robust optical emission polarization in MoS_2 monolayers through selective valley excitation, *Phys. Rev. B* 86(8), 081301 (2012)

278. S. Wu, C. Huang, G. Aivazian, J. S. Ross, D. H. Cobden, and X. Xu, Vapor–solid growth of high optical quality MoS_2 monolayers with near-unity valley polarization, *ACS Nano* 7(3), 2768 (2013)

279. M. Z. Maialle, E. A. de Andrada e Silva, and L. J. Sham, Exciton spin dynamics in quantum wells, *Phys. Rev. B* 47(23), 15776 (1993)

280. E. Palacios, S. Park, S. Butun, L. Lauhon, and K. Aydin, Enhanced radiative emission from monolayer MoS_2 films using a single plasmonic dimer nanoantenna, *Appl. Phys. Lett.* 111(3), 031101 (2017)

281. Y. Zhou, G. Scuri, D. S. Wild, A. A. High, A. Dibos, L. A. Jauregui, C. Shu, K. De Greve, K. Pistunova, A. Y. Joe, et al., Probing dark excitons in atomically thin semiconductors via near-field coupling to surface plasmon polaritons, *Nat. Nanotechnol.* 12(9), 856 (2017)

282. J. Wen, H. Wang, W. Wang, Z. Deng, C. Zhuang, Y. Zhang, F. Liu, J. She, J. Chen, H. Chen, S. Deng, and N. Xu, Room-temperature strong light–matter interaction with active control in single plasmonic nanorod coupled with two-dimensional atomic crystals, *Nano Lett.* 17(8), 4689 (2017)

283. E. Ozbay, Plasmonics: Merging photonics and electronics at nanoscale dimensions, *Science* 311(5758), 189 (2006)

284. J. A. Schuller, E. S. Barnard, W. Cai, Y. C. Jun, J. S. White, and M. L. Brongersma, Plasmonics for extreme light concentration and manipulation, *Nat. Mater.* 9(3), 193 (2010)

285. A. F. Koenderink, A. Alù, and A. Polman, Nanophotonics: Shrinking light-based technology, *Science* 348(6234), 516 (2015)

286. K. F. MacDonald, Z. L. Sámson, M. I. Stockman, and N. I. Zheludev, Ultrafast active plasmonics, *Nat. Photon.* 3(1), 55 (2009)

287. S. Palomba, M. Danckwerts, and L. Novotny, Nonlinear plasmonics with gold nanoparticle antennas, *J. Opt. A* 11(11), 114030 (2009)

288. M. Kauranen and A. V. Zayats, Nonlinear plasmonics, *Nat. Photon.* 6(11), 737 (2012)

289. C. Argyropoulos, N. M. Estakhri, F. Monticone, and A. Alù, Negative refraction, gain and nonlinear effects in hyperbolic metamaterials, *Opt. Express* 21(12), 15037 (2013)

290. P. Bharadwaj, B. Deutsch, and L. Novotny, Optical Antennas, *Adv. Opt. Photon.* 1(3), 438 (2009)

291. L. Novotny and N. Van Hulst, Antennas for light, *Nat. Photon.* 5(2), 83 (2011)

292. A. F. Koenderink, Single-photon nanoantennas, *ACS Photon.* 4(4), 710 (2017)

293. A. Campion and P. Kambhampati, Surface-enhanced Raman scattering, *Chem. Soc. Rev.* 27(4), 241 (1998)

294. A. Otto, I. Mrozek, H. Grabhorn, and W. Akemann, Surface-enhanced Raman scattering, *J. Phys.: Condens. Matter* 4(5), 1143 (1992)

295. P. L. Stiles, J. A. Dieringer, N. C. Shah, and R. P. Van Duyne, Surface-enhanced Raman spectroscopy, *Annu. Rev. Anal. Chem.* 1(1), 601 (2008)

296. E. Palacios, S. Park, L. Lauhon, and K. Aydin, Identifying excitation and emission rate contributions to plasmon-enhanced photoluminescence from monolayer MoS_2 using a tapered gold nanoantenna, *ACS Photon.* 4(7), 1602 (2017)

297. M. Wang, W. Li, L. Scarabelli, B. B. Rajeeva, M. Terrones, L. M. Liz-Marzán, D. Akinwande, and Y. Zheng, Plasmon–trion and plasmon–exciton resonance energy transfer from a single plasmonic nanoparticle to monolayer MoS_2, *Nanoscale* 9(37), 13947 (2017)

298. I. Abid, A. Bohloul, S. Najmaei, C. Avendano, H. L. Liu, R. Péchou, A. Mlayah, and J. Lou, Resonant surface plasmon–exciton interaction in hybrid $MoSe_2$ @Au nanostructures, *Nanoscale* 8(15), 8151 (2016)

299. M. G. Lee, S. Yoo, T. Kim, and Q. H. Park, Large-area plasmon enhanced two-dimensional MoS_2, *Nanoscale* 9(42), 16244 (2017)

300. J. Huang, G. M. Akselrod, T. Ming, J. Kong, and M. H. Mikkelsen, Tailored emission spectrum of 2D semiconductors using plasmonic nanocavities, *ACS Photon.* 5(2), 552 (2017)

301. I. Abid, W. Chen, J. Yuan, A. Bohloul, S. Najmaei, C. Avendano, R. Péchou, A. Mlayah, and J. Lou, Temperature-dependent plasmon–exciton interactions in hybrid Au/$MoSe_2$ nanostructures, *ACS Photon.* 4(7), 1653 (2017)

302. A. Boulesbaa, V. E. Babicheva, K. Wang, I. I. Kravchenko, M.W. Lin, M. Mahjouri-Samani, C. B. Jacobs, A. A. Puretzky, K. Xiao, I. Ivanov, et al., Ultrafast dynamics of metal plasmons induced by 2D semiconductor excitons in hybrid nanostructure arrays, *ACS Photon.* 3(12), 2389 (2016)

303. A. D. Johnson, F. Cheng, Y. Tsai, and C. K. Shih, Giant enhancement of defect-bound exciton luminescence and suppression of band-edge luminescence in monolayer WSe_2–Ag plasmonic hybrid structures, *Nano Lett.* 17(7), 4317 (2017)

304. Z. Li, Y. Li, T. Han, X. Wang, Y. Yu, B. Tay, Z. Liu, and Z. Fang, Tailoring MoS2 exciton-plasmon interaction by optical spin-orbit coupling, *ACS Nano* 11(2), 1165 (2016)

305. H. Y. Jeong, U. J. Kim, H. Kim, G. H. Han, H. Lee, M. S. Kim, Y. Jin, T. H. Ly, S. Y. Lee, Y.G. Roh, et al., Optical gain in MoS_2 *via* coupling with nanostructured substrate: Fabry–Perot interference and plasmonic excitation, *ACS Nano* 10, 8192 (2016)

306. B. Lee, W. Liu, C. H. Naylor, J. Park, S. C. Malek, J. S. Berger, A. C. Johnson, and R. Agarwal, Electrical tuning of exciton–plasmon polariton coupling in monolayer MoS_2 integrated with plasmonic nanoantenna lattice, *Nano Lett.* 17(7), 4541 (2017)

307. M. Hensen, T. Heilpern, S. K. Gray, and W. Pfeiffer, Strong coupling and entanglement of quantum emitters embedded in a nanoantenna-enhanced plasmonic cavity, *ACS Photon.* 5(1), 240 (2018)

308. M. E. Kleemann, R. Chikkaraddy, E. M. Alexeev, D. Kos, C. Carnegie, W. Deacon, A. C. Pury, C. Große, B. Nijs, J. Mertens, et al, Strong-coupling of WSe_2 in ultra-compact plasmonic nanocavities at room temperature, *Nat. Commun.* 8(1), 1296 (2017)

309. D. Zheng, S. Zhang, Q. Deng, M. Kang, P. Nordlander, and H. Xu, Manipulating coherent plasmon–exciton interaction in a single silver nanorod on monolayer WSe_2, *Nano Lett.* 17(6), 3809 (2017)

310. J. Cuadra, D. G. Baranov, M. Wersll, R. Verre, T. J. Antosiewicz, and T. Shegai, Observation of tunable charged exciton polaritons in hybrid monolayer WS_2-plasmonic nanoantenna system, *Nano Lett.* 18(3), 1777 (2018)

311. P. Gonçalves, L. Bertelsen, S. Xiao, and N. A. Mortensen, Plasmon-exciton polaritons in two-dimensional semiconductor/metal interfaces, *Phys. Rev. B* 97(4), 041402 (2018)

312. J. H. Shirley, Solution of the Schrödinger equation with a hamiltonian periodic in time, *Phys. Rev.* 138, B979 (1965)

313. E. J. Sie, J. W. McIver, Y. H. Lee, L. Fu, J. Kong, and N. Gedik, Valley-selective optical Stark effect in monolayer WS_2, *Nat. Mater.* 14(3), 290 (2015)

314. E. J. Sie, C. H. Lui, Y. H. Lee, L. Fu, J. Kong, and N. Gedik, Large, valley-exclusive Bloch–Siegert shift in monolayer WS_2, *Science* 355(6329), 1066 (2017)

315. T. LaMountain, H. Bergeron, I. Balla, T. K. Stanev, M. C. Hersam, and N. P. Stern, Valley-selective optical Stark effect probed by Kerr rotation, *Phys. Rev. B* 97(4), 045307 (2018)

316. S. Sim, D. Lee, M. Noh, S. Cha, C. H. Soh, J. H. Sung, M. H. Jo, and H. Choi, Selectively tunable optical Stark effect of anisotropic excitons in atomically thin ReS_2, *Nat. Commun.* 7, 13569 (2016)

317. A. Mysyrowicz, D. Hulin, A. Antonetti, A. Migus, W. Masselink, and H. Morkoc, "Dressed excitons" in a multiple-quantum-well structure: Evidence for an optical stark effect with femtosecond response time, *Phys. Rev. Lett.* 56(25), 2748 (1986)

318. A. Von Lehmen, D. S. Chemla, J. Heritage, and J. Zucker, Optical Stark effect on excitons in GaAs quantum wells, *Opt. Lett.* 11(10), 609 (1986)

319. W. Knox, D. Chemla, D. Miller, J. Stark, and S. Schmitt-Rink, Femtosecond ac Stark effect in semiconductor quantum wells: Extreme low- and high-intensity limits, *Phys. Rev. Lett.* 62(10), 1189 (1989)

320. D. Chemla, W. Knox, D. Miller, S. Schmitt-Rink, J. Stark, and R. Zimmermann, The excitonic optical stark effect in semiconductor quantum wells probed with femtosecond optical pulses, *J. Lumen.* 44, 233 (1989)

321. E. J. Sie, C. H. Lui, Y. H. Lee, J. Kong, and N. Gedik, Observation of intervalley biexcitonic optical Stark effect in monolayer WS_2, *Nano Lett.* 16(12), 7421 (2016)

322. E. J. Sie, A. J. Frenzel, Y. H. Lee, J. Kong, and N. Gedik, Intervalley biexcitons and many-body effects in monolayer MoS_2, *Phys. Rev. B* 92(12), 125417 (2015)

323. T. Unold, K. Mueller, C. Lienau, T. Elsaesser, and A. D. Wieck, Optical Stark effect in a quantum dot: Ultrafast control of single exciton polarizations, *Phys. Rev. Lett.* 92(15), 157401 (2004)

324. D. D. Awschalom and N. Samarth, in: Semiconductor Spintronics and Quantum Computation, Springer, 2002, pp 147–193

325. J. Gupta, R. Knobel, N. Samarth, and D. Awschalom, Ultrafast manipulation of electron spin coherence, *Science* 292(5526), 2458 (2001)

326. D. Press, T. D. Ladd, B. Zhang, and Y. Yamamoto, Complete quantum control of a single quantum dot spin using ultrafast optical pulses, *Nature* 456(7219), 218 (2008)

327. J. Berezovsky, M. Mikkelsen, N. Stoltz, L. Coldren, and D. Awschalom, Picosecond coherent optical manipulation of a single electron spin in a quantum dot, *Science* 320(5874), 349 (2008)

328. M. Mikkelsen, J. Berezovsky, and D. Awschalom, Ultrafast optical manipulation of single electron spins in quantum dots, *Solid State Commun.* 149(35–36), 1451 (2009)

329. D. Loss and D. P. DiVincenzo, Quantum computation with quantum dots, *Phys. Rev. A* 57(1), 120 (1998)

330. G. Moody, C. K. Dass, K. Hao, C. H. Chen, L. J. Li, A. Singh, K. Tran, G. Clark, X. Xu, G. Berghäuser, E. Malic, A. Knorr, and X. Li, Intrinsic homogeneous linewidth and broadening mechanisms of excitons in monolayer transition metal dichalcogenides, *Nat. Commun.* 6(1), 8315 (2015)

331. P. Dey, J. Paul, Z. Wang, C. Stevens, C. Liu, A. Romero, J. Shan, D. Hilton, and D. Karaiskaj, Optical coherence in atomic-monolayer transition-metal dichalcogenides limited by electron-phonon interactions, *Phys. Rev. Lett.* 116(12), 127402 (2016)

332. L. Bi, J. Hu, P. Jiang, D. H. Kim, G. F. Dionne, L. C. Kimerling, and C. Ross, On-chip optical isolation in monolithically integrated non-reciprocal optical resonators, *Nat. Photon.* 5(12), 758 (2011)

333. E. J. Lenferink, G. Wei, and N. P. Stern, Coherent optical non-reciprocity in axisymmetric resonators, *Opt. Express* 22(13), 16099 (2014)

334. M. Scheucher, A. Hilico, E. Will, J. Volz, and A. Rauschenbeutel, Quantum optical circulator controlled by a single chirally coupled atom, *Science* 354(6319), 1577 (2016)

335. D. Zhong, K. L. Seyler, X. Linpeng, R. Cheng, N. Sivadas, B. Huang, E. Schmidgall, T. Taniguchi, K. Watanabe, M. A. McGuire, W. Yao, D. Xiao, K.M. C. Fu, and X. Xu, Van der Waals engineering of ferromagnetic semiconductor heterostructures for spin and valleytronics, *Sci. Adv.* 3(5), e1603113 (2017)

336. A. Kavokin, G. Malpuech, and M. Glazov, Optical spin Hall effect, *Phys. Rev. Lett.* 95(13), 136601 (2005)

337. O. Bleu, D. Solnyshkov, and G. Malpuech, Optical valley Hall effect based on transitional metal dichalcogenide cavity polaritons, *Phys. Rev. B* 96(16), 165432 (2017)

338. T. Karzig, C. E. Bardyn, N. H. Lindner, and G. Refael, Topological polaritons, *Phys. Rev. X* 5(3), 031001 (2015)

339. Y. V. Kartashov and D. V. Skryabin, Bistable topological insulator with exciton-polaritons, *Phys. Rev. Lett.* 119(25), 253904 (2017)

340. N. Gippius, I. Shelykh, D. Solnyshkov, S. Gavrilov, Y. G. Rubo, A. Kavokin, S. Tikhodeev, and G. Malpuech, Polarization multistability of cavity polaritons, *Phys. Rev. Lett.* 98(23), 236401 (2007)

341. T. Paraïso, M. Wouters, Y. Léger, F. Morier-Genoud, and B. Deveaud-Plédran, Multistability of a coherent spin ensemble in a semiconductor microcavity, *Nat. Mater.* 9(8), 655 (2010)

342. V. M. Menon, L. I. Deych, and A. A. Lisyansky, Towards polaritonic logic circuits, *Nat. Photon.* 4(6), 345 (2010)